New band mechanism of doubly-odd nuclei around mass 130

K. Higashiyama,[1,*] N. Yoshinaga,[2,†] and K. Tanabe[2]
[1]*Department of Physics, University of Tokyo, Hongo, Tokyo 113-0033, Japan*
[2]*Department of Physics, Saitama University, Saitama City 338-8570, Japan*
(Received 23 February 2005; published 22 August 2005)

The nuclear structure of the $\Delta I = 1$ doublet bands in doubly-odd nuclei ^{130}Cs, ^{132}Cs, ^{132}La, and ^{134}La is studied in terms of a pair-truncated shell model, in which the collective nucleon pairs with angular momenta of zero and two are its basic ingredients. The effective interactions consist of single-particle energies and monopole and quadrupole pairing plus quadrupole-quadrupole interactions, whose strengths are determined so as to describe the level schemes of even-even nuclei in the mass $A \sim 130$ region. The calculation reproduces well the energy levels of the doublet bands and the electromagnetic transitions, especially the staggering of the ratios $B(M1; I \to I-1)/B(E2; I \to I-2)$ for the yrast states. Through the analysis of the wave functions, the doublet bands turn out to be made of different angular momentum configurations of an unpaired neutron and an unpaired proton, weakly coupled with the quadrupole collective excitations of the even-even part of the nucleus.

DOI: 10.1103/PhysRevC.72.024315 PACS number(s): 21.60.Cs, 21.60.Ev, 27.60.+j

I. INTRODUCTION

The nuclei in the mass $A \sim 130$ region that have just more than 50 protons and just fewer than 82 neutrons show various intriguing phenomena, one of which is the γ instability caused by the prolatelike mass distribution of valence proton particles and oblatelike mass distribution of valence neutron holes, respectively. The γ instability of the $A \sim 130$ even-even nuclei is manifested by the energy staggering of even-odd spin states in the quasi-γ bands and by some forbidden transitions between the yrast and the quasi-γ bands [1,2]. Another interesting phenomenon is the backbending [3–6]. The Fermi level lies in the $0h_{11/2}$ orbital for neutrons, and a weak rotation causes the spin alignment of quasiparticles in this orbital. In addition, we observe a number of high-spin isomers [7–9], which are related to the validity of the seniority scheme for the single-$0h_{11/2}$ orbital.

In the past two decades, a number of systematic studies on these nuclei were performed. The interacting boson model (IBM) has been widely used for the study of the low-lying states [10]. In this model, quadrupole collective excitations are described in terms of angular momenta zero (s) and two (d) bosons. Extensive studies were carried out for the low-lying states of the $A \sim 130$ even-even nuclei [1,2,11–16], and the energy spectra and the electromagnetic transitions were well approximated by the IBM Hamiltonian with the O(6) dynamical symmetry.

The pair-truncated shell model (PTSM) [17–24] provides another practical scheme for a microscopic description of collective motion in medium and heavy nuclei in terms of fermionic collective pairs. In the simplest version of the PTSM, i.e., the *SD* version of the PTSM, even-even nuclear states are constructed by angular momenta zero (S) and two (D) collective pairs. Based on this framework, systematic studies were carried out for the even-even and the odd-mass nuclei in the mass $A \sim 130$ region [23]. In this work, energy spectra of both the yrast and the quasi-γ bands for even-even isotopes $_{54}$Xe, $_{56}$Ba, $_{58}$Ce, and $_{60}$Nd were well reproduced, along with the intraband and the interband $B(E2)$ values. The same set of interactions was applied to odd-mass nuclei, and an excellent agreement with experimental data was achieved for both the energy spectra and the magnetic moments.

One of the most intriguing phenomena in medium and heavy nuclei is the systematic appearance of the $\Delta I = 1$ doublet bands, which are observed to be almost degenerate in energy as the low-lying bands in some doubly-odd nuclei. For instance, the bandhead states of these $\Delta I = 1$ doublet bands appear at excitation energies of 0.975, 1.131, and 0.775 MeV in $^{130}_{55}$Cs [25], ^{132}Cs [26,27], and $^{132}_{57}$La [27,28], respectively. Such pairs of bands built on the single-particle states of a valence neutron and a valence proton in the same unique-parity orbital $0h_{11/2}$ were observed in recent experimental studies of doubly-odd nuclei around the mass 130. In Ref. [29], new sideband partners of the yrast bands were identified for the doubly-odd $N = 75$ isotones. Later the $\Delta I = 1$ doublet bands and the even-odd staggering of the ratios $B(M1; I \to I-1)/B(E2; I \to I-2)$ were observed for $^{136}_{61}$Pm and $^{138}_{63}$Eu [30]. Furthermore, for many doubly-odd nuclei, several members of the doublet bands have been accumulated, and a similar trend has been ascertained for both the energy levels and the $B(M1)/B(E2)$ ratios [31–37].

These doublet bands had been interpreted as the manifestation of "chirality" by Frauendorf and Meng, based on the three-dimensional tilted axis cranking (TAC) model [38]. In their picture, the chiral mechanism is explained as follows. When three angular momenta of the even-even core, the unpaired neutron, and the unpaired proton are perpendicular to each other, they can form either a left-handed or a right-handed geometrical configuration, which cannot be transformed into one another by rotation. These left-handed and right-handed configurations constitute the chirality in the intrinsic body-fixed frame. Restoration of the chiral symmetry in the laboratory frame results in two bands in which the states of the same spin and parity are almost degenerate in energy.

*Electronic address: higashi@nt.phys.s.u-tokyo.ac.jp
†Electronic address: yoshinaga@phy.saitama-u.ac.jp

 ©2005 The American Physical Society

Among many theoretical studies on the $\Delta I = 1$ doublet bands, the TAC model was first employed to calculate the excitation-energy patterns and electromagnetic properties of the doubly-odd nuclei in the mass $A \sim 130$ region [29,30,36,38,39]. The calculations reproduced rather well the experimental excitation energies, but could not explain the staggering of the experimental $B(M1)/B(E2)$ ratios in the yrast band. Theoretical investigations of the doublet bands were carried out also within the framework of the phenomenological core-particle-hole coupling model [34,35] and the particle-rotor model (PRM) [32,40,41], and these results supported the interpretation of the doublet bands of the chiral structure. These models, however, disregarded the intrinsic degrees of freedom of the even-even core, i.e., in these models, an even-even core was assumed to be "a triaxial rotor" with definite triaxial deformation and irrotational-flow-like moment of inertia, and a doubly-odd nucleus was described by an unpaired neutron and an unpaired proton in the $0h_{11/2}$ orbitals, surrounding the triaxial rotor. In contrast, it is well known that the even-even nuclei in the mass $A \sim 130$ region are γ unstable in low-lying states, and a proper treatment of the core is essential for a description of their structures. Our attempt in this paper is to take an explicit account of the single-particle degrees of freedom of the even-even core in order to describe such a variety of band structures in these doubly-odd nuclei.

For the description of doubly-odd nuclei, the IBM was extended to include the single-particle degrees of freedom for both neutrons and protons [42]. The extended model, the so-called interacting boson fermion-fermion model (IBFFM), was applied to the doubly-odd nuclei in the mass $A \sim 130$ region to reproduce the complicated level schemes and the electromagnetic properties [43–45]. The IBFFM was applied also to the doublet bands in $^{134}_{59}$Pr [46]. Through the analysis of the wave functions and the transitions, it was concluded that the yrast band was fundamentally built on the ground-state band of the even-even triaxial core, whereas the yrare band was mainly built on the quasi-γ band of the core. The IBFFM was successful in describing the low-lying states of the doubly-odd nuclei, though the model cannot explicitly deal with the effect of the Pauli principle between the boson core and the fermionic unpaired particles.

Like the IBM, the PTSM was extended for a microscopic description of doubly-odd nuclei. The $\Delta I = 1$ doublet bands for ^{132}La [47] and ^{134}La [48–50] were analyzed in terms of the extended PTSM, and a good agreement with experiment was achieved for the energy levels of the bands. The calculation reproduced well the observed $B(M1)/B(E2)$ ratios for ^{134}La. Through the analysis of the behavior of the wave functions, it was found that the level scheme of the $\Delta I = 1$ doublet bands does not arise from the chiral structure, but from different angular momentum configurations of the unpaired neutron and the unpaired proton in the $0h_{11/2}$ orbitals, weakly coupled with the quadrupole collective excitations of the even-even core. If we follow the $\Delta I = 1$ sequence from the ground state with the $\nu h_{11/2} \otimes \pi h_{11/2}$ configuration, the angular momenta of the neutron and the proton open and close like scissors. This scissorslike motion is called "chopsticks motion" hereafter. The chopsticks motion, representing the restless movement of two angular momenta of the unpaired neutron and the unpaired proton, is quite different from the shears mechanism. In the latter picture, the blades of the shears, representing two angular momenta of valence neutrons and valence protons, gradually close as spin I increases, and the $B(M1)$ transition strength monotonically decreases with increasing spin I. On the other hand, in the chopsticks motion, the chopsticks open and close repeatedly as spin I increases, and it provides the characteristic feature of the staggered $M1$ transitions along the yrast band.

In this paper, we perform systematic analysis of the $\Delta I = 1$ doublet bands with excitation energies of about 1 MeV for the $A \sim 130$ doubly-odd nuclei in terms of the PTSM. We employ the monopole and quadrupole pairing plus quadrupole-quadrupole ($P+QQ$) interaction as an effective interaction, and take the full shell-model spaces from the nucleon number 50–82 configuration for both neutrons and protons. The optimum set of the interaction strengths was already determined from the experimental energy levels for the even-even nuclei, $^{128-132}$Xe, $^{130-134}$Ba, and $^{132-136}$Ce [23]. Carrying out systematic calculations for the doubly-odd nuclei, ^{130}Cs, ^{132}Cs, ^{132}La, and ^{134}La, we compare the theoretical energy spectra and the electromagnetic properties with the corresponding experimental data and examine the physical contents of the theoretical wave functions.

The paper is organized as follows. In Sec. II, we give a brief outline of the PTSM and its effective interactions in the model space. In Sec. III, we present numerical studies on the even-even nuclei, ^{130}Xe, ^{132}Xe, ^{132}Ba, and ^{134}Ba. In Sec. IV, the same set of the interactions determined from the even-even nuclei is applied to the doubly-odd nuclei, ^{130}Cs, ^{132}Cs, ^{132}La, and ^{134}La. In Sec. V, we analyze the wave functions of the $\Delta I = 1$ doublet bands. In Sec. VI, we conclude the paper with a summary. In the appendix, we give explicit expressions for some important physical quantities in a one-neutron and one-proton system in the same single-j orbital.

II. THEORETICAL FRAMEWORK

The impressive success of the IBM suggests that nucleon collective pairs with low angular momenta play dominant roles in the nuclear collective motion. It is natural to expect that the *SD* pair-truncation scheme works well in describing low-lying states. As such an approach, the *SD* version of the PTSM was proposed [17–24]. In this model, the shell-model basis is restricted to the *SD* subspace with S and D collective pairs. The S and D pair-creation operators, as building blocks of the model, are defined as

$$S^\dagger = \sum_j \alpha_j A_0^{\dagger(0)}(jj), \tag{1}$$

$$D_M^\dagger = \sum_{j_1 j_2} \beta_{j_1 j_2} A_M^{\dagger(2)}(j_1 j_2), \tag{2}$$

where the structure coefficients α and β are determined by a variation in each nucleus as in Ref. [18]. The creation operator of a pair of nucleons in the orbitals j_1 and j_2 with a total

angular momentum I and its projection M is written by

$$A^{\dagger(I)}_M(j_1 j_2) = \sum_{m_1 m_2} (j_1 m_1 j_2 m_2 | IM)\, c^\dagger_{j_1 m_1} c^\dagger_{j_2 m_2} = \left[c^\dagger_{j_1} c^\dagger_{j_2}\right]^{(I)}_M, \quad (3)$$

where $c^\dagger_{jm}$ represents either a neutron-hole creation operator or a proton-particle creation operator in the orbital jm. Using the S and D pair-creation operators, we construct a many-body SD pair state by applying creation operators on the closed-shell core $|-\rangle$ as

$$|S^{n_s} D^{n_d} I\eta\rangle = (S^\dagger)^{n_s} (D^\dagger)^{n_d} |-\rangle, \quad (4)$$

where I is an angular momentum of the nuclear state and η an additional quantum number required for completely specifying the state. Here, the necessary angular momentum coupling is exactly carried out, but abbreviated for notational simplicity. The n_s and n_d represent the numbers of the S and D pairs, respectively. Thus the number of valence nucleons, $2n_s + 2n_d$, is a fixed constant for a given nucleus. To describe open-shell nuclei, we use the preceding SD pair states in both neutron and proton spaces and couple them to the state with a total spin I. Thus the many-body wave function of the even-even nucleus can be written as

$$|\Phi(I\eta)\rangle = \left[\left|S^{\bar{n}_s}_\nu D^{\bar{n}_d}_\nu I_\nu \eta_\nu\right\rangle \otimes \left|S^{n_s}_\pi D^{n_d}_\pi I_\pi \eta_\pi\right\rangle\right]^{(I)}, \quad (5)$$

where $\bar{n}_s$ and $\bar{n}_d$ represent the numbers of neutron-hole S pairs and D pairs, respectively, and n_s and n_d correspond to those for proton pairs. The $2\bar{n}_s + 2\bar{n}_d$ $(=\bar{N}_\nu)$ and $2n_s + 2n_d$ $(=N_\pi)$ are the total numbers of valence neutron holes and proton particles, respectively. Later the state in Eq. (5) will constitute the even-even core of the doubly-odd nuclear state.

To describe an odd-nucleon state, we need to extend the model to include an unpaired nucleon in addition to the SD pair state [21,23]. When the nucleon creation operator $c^\dagger_{jm}$ is applied to the SD pair state, the odd-nucleon state, i.e., the SD pairs plus one particle state, is constructed as

$$|j S^{n_s} D^{n_d} I\eta\rangle = [c^\dagger_j | S^{n_s} D^{n_d} I'\eta\rangle]^{(I)}, \quad (6)$$

where I and η denote the same as before, and $2n_s + 2n_d + 1$ is the number of valence nucleons. Because of this extension, the PTSM can treat even-even, odd-mass, and doubly-odd nuclei on the same footing. As in the case of the even-even nucleus, the many-body wave function of a doubly-odd nucleus is expressed as follows:

$$|\Phi(I\eta)\rangle = \left[\left|j_\nu S^{\bar{n}_s}_\nu D^{\bar{n}_d}_\nu I_\nu \eta_\nu\right\rangle \otimes \left|j_\pi S^{n_s}_\pi D^{n_d}_\pi I_\pi \eta_\pi\right\rangle\right]^{(I)}, \quad (7)$$

where $2\bar{n}_s + 2\bar{n}_d + 1$ $(= \bar{N}_\nu)$ and $2n_s + 2n_d + 1$ $(= N_\pi)$ are the total numbers of valence neutron holes and proton particles, respectively. In the present calculation, the number of proton pairs is fixed at two $(n_s + n_d = 2)$ for Xe and Cs isotopes and three $(n_s + n_d = 3)$ for Ba and La isotopes. Similarly, the number of neutron pairs is fixed at two $(\bar{n}_s + \bar{n}_d = 2)$ for $N = 78$ isotones and three $(\bar{n}_s + \bar{n}_d = 3)$ for $N = 76$ isotones. Through a Schmidt orthonormalization procedure, the states with a total spin I are orthonormalized to each other.

In the present study, we employ the P+QQ interaction as an effective interaction, which is frequently used for medium and heavy nuclei. The effective shell-model Hamiltonian is written as

$$H = H_\nu + H_\pi + H_{\nu\pi}, \quad (8)$$

where H_ν, H_π, and $H_{\nu\pi}$ represent the neutron interaction, the proton interaction, and the neutron-proton interaction, respectively. The interaction among like nucleons H_τ $(\tau = \nu$ or $\pi)$ consists of spherical single-particle energies, monopole-pairing (MP), quadrupole-pairing (QP), and quadrupole-quadrupole (QQ) interactions:

$$H_\tau = \sum_{jm} \varepsilon_{j\tau} c^\dagger_{jm\tau} c_{jm\tau} - G_{0\tau} P^{\dagger(0)}_\tau P^{(0)}_\tau - G_{2\tau} P^{\dagger(2)}_\tau \cdot \tilde{P}^{(2)}_\tau - \kappa_\tau : Q_\tau \cdot Q_\tau :, \quad (9)$$

where :: denotes normal ordering. The monopole-pairing operator $P^{\dagger(0)}_\tau$, the quadrupole-pairing operators $P^{\dagger(2)}_{M\tau}$, $\tilde{P}^{(2)}_{M\tau}$, and the quadrupole operator $Q_{M\tau}$ are defined as

$$P^{\dagger(0)}_\tau = \sum_j \frac{\sqrt{2j+1}}{2} A^{\dagger(0)}_{0\tau}(jj), \quad (10)$$

$$P^{\dagger(2)}_{M\tau} = \sum_{j_1 j_2} Q_{j_1 j_2} A^{\dagger(2)}_{M\tau}(j_1 j_2), \quad (11)$$

$$\tilde{P}^{(2)}_{M\tau} = (-1)^M P^{(2)}_{-M\tau}, \quad (12)$$

$$Q_{M\tau} = \sum_{j_1 j_2} Q_{j_1 j_2} \left[c^\dagger_{j_1\tau} \tilde{c}_{j_2\tau}\right]^{(2)}_M, \quad (13)$$

$$[\tilde{c}_{jm\tau} = (-1)^{j-m} c_{j-m\tau}],$$

$$Q_{j_1 j_2} = -\frac{\langle j_1 || r^2 Y^{(2)} || j_2\rangle}{\sqrt{5}}, \quad (14)$$

where $A^{\dagger(I)}_{M\tau}$ stands for the pair-creation operator given by Eq. (3). We assume that the interaction between neutrons and protons $H_{\nu\pi}$ is just expressed as the QQ interaction:

$$H_{\nu\pi} = -\kappa_{\nu\pi} Q_\nu \cdot Q_\pi, \quad (15)$$

where Q_τ is written in terms of proton-particle or neutron-hole operators. As for the single-particle basis states, we employ the harmonic-oscillator basis states with the oscillator parameter $b = \sqrt{\hbar/M\omega}$. The detailed framework of the PTSM is presented in Ref. [23].

III. NUMERICAL RESULTS OF EVEN-EVEN NUCLEI

In the mass $A \sim 130$ region, several valence proton particles and valence neutron holes are coupled to the doubly magic ^{132}Sn core. Because they occupy the $0g_{7/2}$, $1d_{5/2}$, $1d_{3/2}$, $0h_{11/2}$, and $2s_{1/2}$ orbitals, the shell-model space used in our calculation includes full one-major shell-model spaces from the nucleon-number 50–82 configuration for both neutrons and protons, in which valence neutrons are treated as holes and valence protons as particles. The adopted single-particle energies, listed in Table I, are extracted from experimental excitation energies in Refs. [51–53].

TABLE I. Adopted single-particle energies (in MeV) for neutron holes and proton particles, which are extracted from experimental data [51–53].

j	$2s_{1/2}$	$0h_{11/2}$	$1d_{3/2}$	$1d_{5/2}$	$0g_{7/2}$
ε_ν	0.332	0.242	0.000	1.655	2.434
ε_π	2.990	2.793	2.708	0.962	0.000

For these valence spaces, we use the P+QQ interactions, whose strengths were determined by a least-squares fit of the low-lying energy levels as for the even-even nuclei, $^{128-132}$Xe, $^{130-134}$Ba, and $^{132-136}$Ce in Ref. [23]. To reproduce overall spectra of the preceding nuclei, the linear dependence of the interaction strengths on the valence neutron and/or proton numbers was introduced. The determined set of interactions is as follows (G_0 of MP interaction in MeV and G_2 of QP interaction and κ of QQ interaction in MeV/b^4):

$$\begin{aligned} G_{0\nu} &= 0.160 - 0.010\bar{N}_\nu, \\ G_{2\nu} &= 0.017 + 0.0005N_\pi, \\ \kappa_\nu &= 0.075 - 0.0015N_\pi, \\ G_{0\pi} &= 0.200 - 0.010\bar{N}_\nu - 0.005N_\pi, \\ G_{2\pi} &= 0.010 + 0.001N_\pi, \\ \kappa_\pi &= 0.014 + 0.006N_\pi, \\ \kappa_{\nu\pi} &= -0.044 - 0.002\bar{N}_\nu. \end{aligned} \tag{16}$$

Here $\bar{N}_\nu$ represents the number of neutron holes and N_π the number of proton particles.

In Fig. 1, the theoretical energy spectra of the PTSM are compared with experimental data for even-even nuclei, ^{130}Xe, ^{132}Xe, ^{132}Ba, and ^{134}Ba, up to spin 8. The energy levels of the even-spin yrast band for ^{130}Xe, ^{132}Xe, and ^{134}Ba are well reproduced. The staggering patterns of the energy levels in the quasi-γ bands are also described well, indicating the γ instability in the low-lying states. For ^{132}Ba, the model gives good agreement with experimental data, including high-spin states. The theoretical $E2$ transitions and branching ratios also agree well with experimental data. Some other details were presented in Ref. [23].

IV. NUMERICAL RESULTS OF DOUBLY-ODD NUCLEI

A. Energy spectra

The $\Delta I = 1$ doublet bands reported in recent experiments of the doubly-odd nuclei in the mass $A \sim 130$ region are assigned to be built on the $\nu h_{11/2} \otimes \pi h_{11/2}$ configuration. Thus we take into account the $\nu h_{11/2} \otimes \pi h_{11/2}$ configuration coupled with the SD pair states. As for the single-particle energies and the strengths of the effective interaction, we use the same values that were determined from the energy spectra of the even-even nuclei as in Table I and Eqs. (16).

In experiment three $\Delta I = 1$ bands are assigned to be built on the $\nu h_{11/2} \otimes \pi h_{11/2}$ configuration for ^{132}Cs (even-even core: ^{132}Xe). In Fig. 2, the experimental energy spectrum is compared with the PTSM result. The PTSM reproduces quite well the energy levels for bands 1 and 2. However, the theoretical result is not satisfactory enough to describe the energy levels of band 3, where level spacings between the $\Delta I = 1$ states are smaller compared with those of the other bands (bands 1 and 2). The nucleus ^{132}Cs has fewer valence neutrons and protons compared with the other nuclei, ^{130}Cs, ^{132}La, and ^{134}La. The quadrupole collectivity is not so pronounced, and the single-particle nature still dominates. For an accurate description of band 3, we may need to take into account some other effects such as a hexadecapole degree of freedom.

In Fig. 3, the experimental energy levels for ^{130}Cs (even-even core: ^{130}Xe) are compared with the PTSM results. Concerning the yrast states, calculated energy levels are in good agreement with experiment. There is no experimental evidence for the 8_1^+ state, but the theoretical 8_1^+ state is in between 9_1^+ and 10_1^+ states. For the yrare states, the PTSM calculation reproduces the observed levels at correct positions, though the model predicts a few low-spin states that are not experimentally observed.

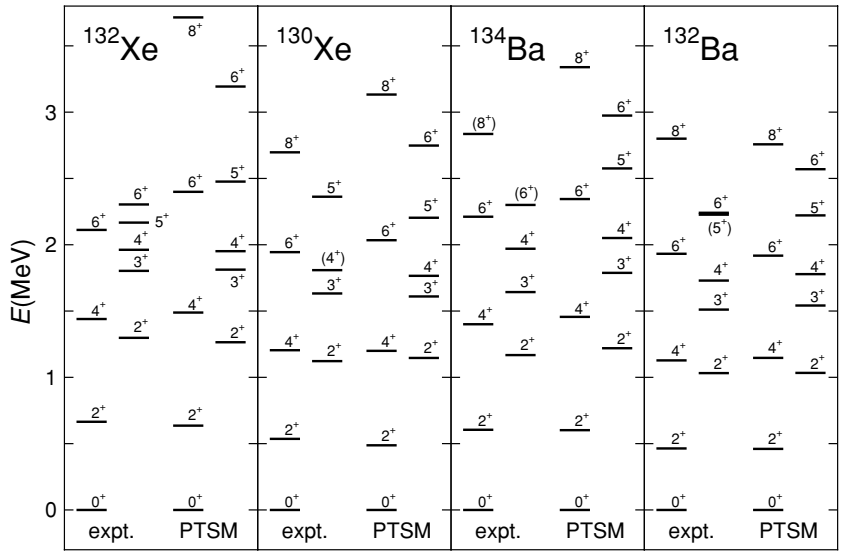

FIG. 1. Comparison of the experimental energy levels (expt.) with those of the PTSM for ^{130}Xe, ^{132}Xe, ^{132}Ba, and ^{134}Ba. The level sequences on the right represent the quasi-γ band, and the level sequences on the left the yrast band. Experimental data are taken from Refs. [6,54–57].

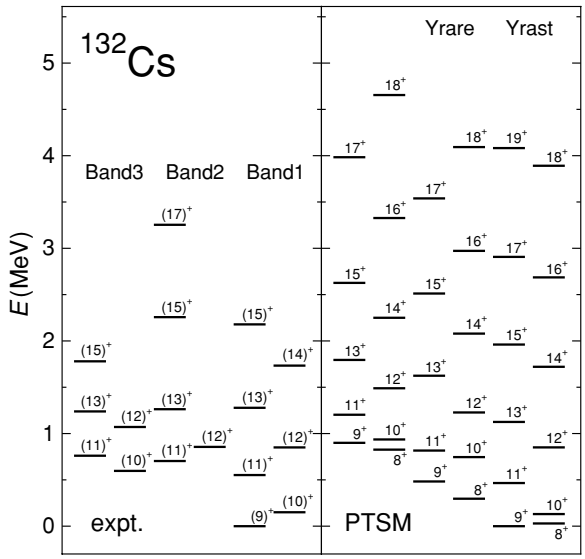

FIG. 2. Comparison of the experimental energy levels (expt.) with those of the PTSM for ^{132}Cs. The two level sequences of $\Delta I = 1$ on the right represent the yrast band, and the two level sequences of $\Delta I = 1$ on the middle, the yrare band. The two levels on the left denote the third lowest energy states for each total spin I. Experimental data are taken from Ref. [35].

The energy spectra for ^{134}La (even-even core: ^{134}Ba) are shown in Fig. 4. The model reproduces well the energy levels of low-energy states, and the level sequence of 8_1^+, 9_1^+, and 10_1^+ states is predicted similarly to those of ^{130}Cs and ^{132}Cs. For the higher-energy states with spins greater then 18, the theoretical level spacings between $\Delta I = 2$ states are larger compared with those of experiment. Such high-spin states may be complicated in structure, so that the S and D collective pairs are insufficient to describe the even-even cores of the high-spin states. For a more accurate description of these states, we may need higher-spin pairs, such as the H pairs, which are composed of two nucleons in the $0h_{11/2}$ orbitals [22,24].

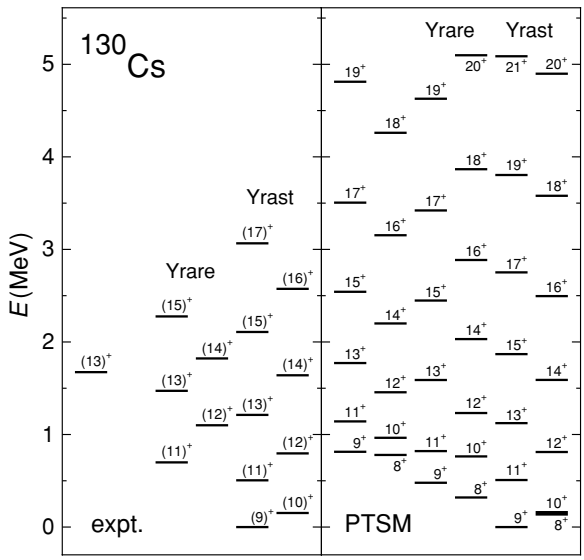

FIG. 3. Same figure as in Fig. 2, but for ^{130}Cs. Experimental data are taken from Ref. [35].

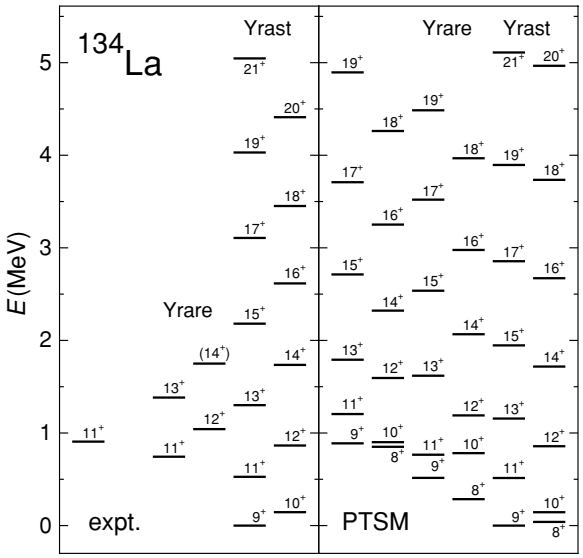

FIG. 4. Same figure as in Fig. 2, but for ^{134}La. Experimental data are taken from Ref. [33].

Figure 5 shows the energy spectra of ^{132}La (even-even core: ^{132}Ba). The level ordering of the 8_1^+ and 9_1^+ states is reversely predicted in the PTSM, though the ground state of 8_1^+ and the first excited state of 9_1^+ with the $\nu h_{11/2} \otimes \pi h_{11/2}$ configuration are almost degenerate in experiment. For the other yrast and yrare states, the PTSM reproduces well the energy levels. Especially, for high-spin states we obtain a better agreement with the experimental data compared with the other nuclei. More numbers of the S and D pairs are available for this nucleus, so that high-energy states are now well described.

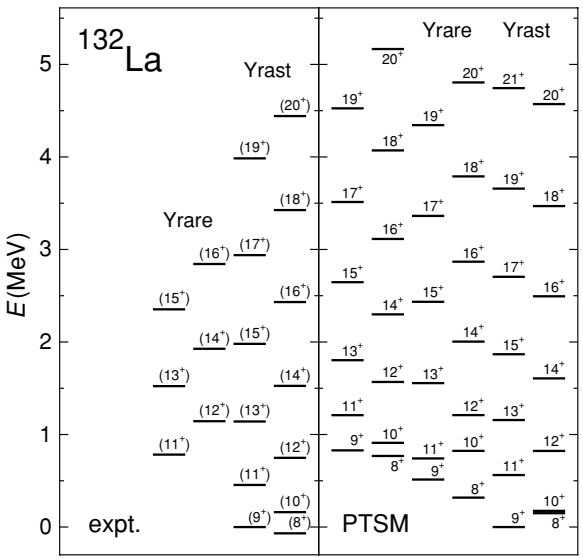

FIG. 5. Same figure as in Fig. 2, but for ^{132}La. Experimental data are taken from Ref. [34].

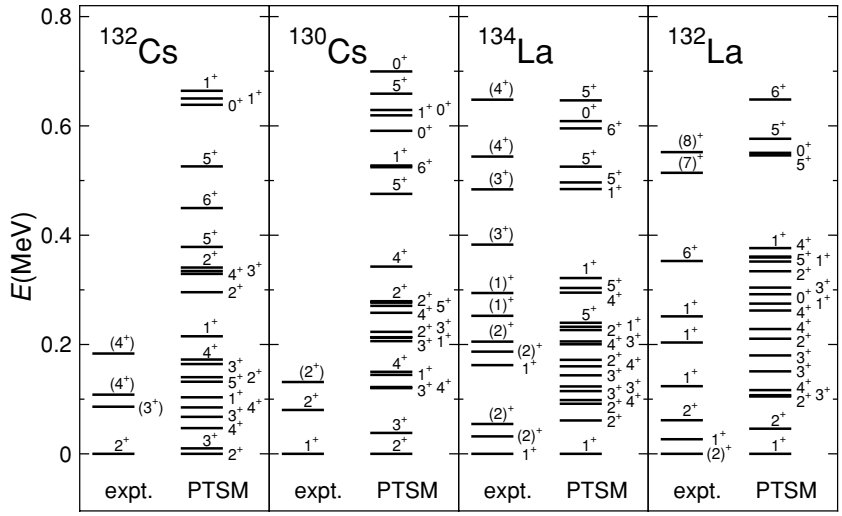

FIG. 6. Comparison of the experimental energy levels (expt.) with those of the PTSM for ^{130}Cs, ^{132}Cs, ^{132}La, and ^{134}La. Experimental data are taken from Refs. [25–27,58,59].

B. Energy spectra of other low-lying positive-parity states

In this paper our main concern is the structure of the yrast and yrare states built from the $\nu h_{11/2} \otimes \pi h_{11/2}$ configuration. However, one of the advantages of our framework is to simultaneously describe the low-lying states that are not built from the $\nu h_{11/2} \otimes \pi h_{11/2}$ configuration. In Fig. 6, theoretical energy levels with positive parity are compared with the experimental data up to 700 keV excitation for ^{130}Cs, ^{132}Cs, ^{132}La, and ^{134}La. In experiment, the ground states are assigned to have positive parity for ^{130}Cs, ^{132}Cs, and ^{134}La, whereas in ^{132}La the ground state is assigned to have negative parity, and the lowest state with positive parity, the $(2)^+$ state, has an excitation energy of 155 keV.

Concerning ^{132}Cs and ^{134}La, calculated energy levels are in good agreement with experiment. In particular, spins of the ground states are exactly reproduced. For ^{130}Cs, the 1_1^+ state appears higher in energy than the experimental one, but there exists a one-to-one correspondence between the theoretical and experimental levels for the 1_1^+ and 2_1^+ states. For ^{132}La, the ordering of the 1_1^+ and 2_1^+ states is reversely predicted, but the PTSM calculation reproduces quite well the positions of the energy levels for the 2_1^+, 1_1^+, 2_2^+, and 1_2^+ states.

The PTSM also gives the relative energies between the ground states with positive parity and the states with the $\nu h_{11/2} \otimes \pi h_{11/2}$ configuration, which are not shown in the figure. The experimental yrast bands based on the $\nu h_{11/2} \otimes \pi h_{11/2}$ configuration start at excitation energies of 0.975, 1.131, and 0.775 MeV in ^{130}Cs [25], ^{132}Cs [26,27], and ^{132}La [27,28], respectively. In the PTSM, the ground states with the $\nu h_{11/2} \otimes \pi h_{11/2}$ configuration are located at excitation energies of 1.79, 1.75, 1.34, and 1.29 MeV in ^{130}Cs, ^{132}Cs, ^{132}La, and ^{134}La, respectively, which are rather high in energy compared with experiment.

Through the analysis of odd-mass nuclei, we have already noted that our model Hamiltonian is not satisfactory enough to reproduce the low-lying energy levels of odd-mass nuclei [23]. For a reproduction of the relative positions of the states with the $\nu h_{11/2} \otimes \pi h_{11/2}$ configuration, we may need either to shift the single-particle energy of the $0h_{11/2}$ orbital relative to the other orbitals and/or to include an octupole interaction, which is missing in the present study.

C. Relative $M1$ and $E2$ transitions

In what follows we calculate the ratios $B(M1; I \to I-1)/B(E2; I \to I-2)$ for the yrast states with the $\nu h_{11/2} \otimes \pi h_{11/2}$ configuration and the ratios $B(M1; I \to I-1)_{\rm In}/B(M1; I \to I-1)_{\rm Out}$ for the transitions from the yrare states, as these are the only measured transitions in experiment.

The $M1$ transition operator is defined as

$$T(M1;\mu) = \mu_N \sqrt{\frac{3}{4\pi}} \sum_{\tau=\nu,\pi} [g_{\ell\tau}\, \boldsymbol{j}_\tau + (g_{s\tau} - g_{\ell\tau})\boldsymbol{s}_\tau]_\mu, \quad (17)$$

where μ_N ($= e\hbar/2mc$) is the nuclear magneton, $g_{\ell\tau}$ ($g_{s\tau}$) is the g factor for orbital angular momentum (spin). The operators $\boldsymbol{j}_\tau$ and $\boldsymbol{s}_\tau$ stand for the angular momentum and the spin operators, respectively. The adopted gyromagnetic ratios for the orbital angular momentum are $g_{\ell\nu} = 0.00$ and $g_{\ell\pi} = 1.00$ and those for spin are $g_{s\nu} = -2.68$ and $g_{s\pi} = 3.91$, which are free nucleon g factors attenuated by a factor of 0.7.

The $E2$ transition operator is defined as

$$T(E2;\mu) = e_\nu Q_{\nu\mu} + e_\pi Q_{\pi\mu}, \quad (18)$$

where e_τ represents the effective charge of the nucleon and the operator Q_τ is the quadrupole operator defined by Eq. (13) with the oscillator parameter $b = 1.005A^{1/6}$ fm. The effective charges are assumed to follow the conventional relation $e_\nu = -\delta e$ and $e_\pi = (1+\delta)e$ [60], and the adopted values are $\delta = 0.60 + 0.05(\bar{N}_\nu + N_\pi)$, which are taken from Ref. [23].

In Fig. 7, the theoretical $B(M1)/B(E2)$ ratios for the yrast states are compared with experiment. The large-amplitude staggering of the $B(M1)/B(E2)$ ratios are in excellent agreement with experimental data, except for the 16_1^+ state of ^{134}La and for the 17_1^+ state of ^{132}Cs. The anomalous behavior at spin 16 of ^{134}La may be attributed to a band crossing between the yrast and the yrare bands. As an indication, irregular level sequences in the yrast bands were reported on the neighboring Pr isotopes [44,45,61]. In particular, the positive-parity yrast

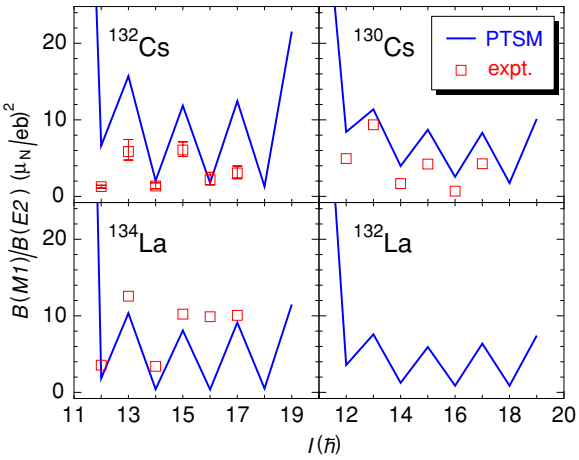

FIG. 7. (Color online). Comparison of the calculated $B(M1)/B(E2)$ ratios for the yrast states of ^{130}Cs, ^{132}Cs, ^{132}La, and ^{134}La with experiment. Experimental data are taken from Refs. [33,35,36]. No experimental data are available for ^{132}La.

bands with the $\nu h_{11/2} \otimes \pi h_{11/2}$ configuration in ^{134}Pr exhibit the irregular level sequences because of a band crossing at spin 15 and 16 [61]. The anomalous behavior at spin 17 of ^{132}Cs may also be explained by the band crossing between the yrast and the yrare bands. As ^{132}Cs shows a complicated level structure arising from the excitations of both single-particle and collective degrees of freedom, this anomalous behavior might be caused by another mechanism.

In Fig. 8, the theoretical $B(M1)_{\mathrm{In}}/B(M1)_{\mathrm{Out}}$ ratios for the transitions from the yrare states are compared with experiment. The $B(M1)_{\mathrm{In}}$ indicates the $M1$ transition between yrare states, and $B(M1)_{\mathrm{Out}}$ indicates the $M1$ transition from yrare to yrast states. In ^{130}Cs the model reproduces the staggering feature, but slightly underestimates its value at spin 13. In ^{132}Cs there is a large disagreement between the experimental and calculated $B(M1)_{\mathrm{In}}/B(M1)_{\mathrm{Out}}$ ratios, but this discrepancy

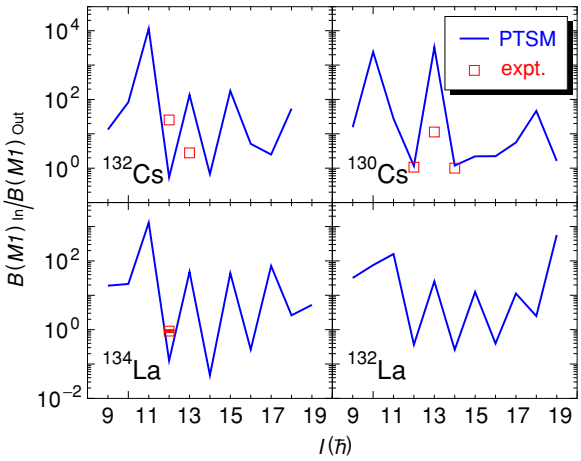

FIG. 8. (Color online). Comparison of the calculated $B(M1)_{\mathrm{In}}/B(M1)_{\mathrm{Out}}$ ratios for the yrare states of ^{130}Cs, ^{132}Cs, ^{132}La, and ^{134}La with the experimental data. Experimental data are taken from Refs. [33,35]. No experimental data are available for ^{132}La.

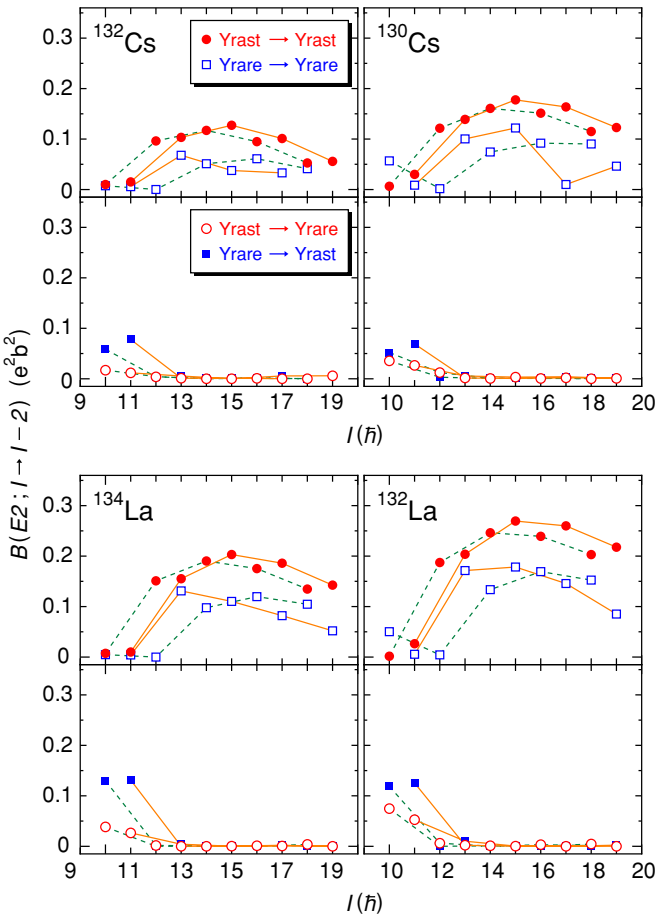

FIG. 9. (Color online). The theoretical $B(E2)$ values for ^{132}Cs, ^{130}Cs, ^{134}La, and ^{132}La. The filled circles, open squares, open circles, and filled squares represent the transitions between yrast states, between yrare states, from yrast to yrare states, and from yrare to yrast states, respectively. Solid curves indicate the transitions between the odd-spin states, and dotted curves, the transitions between even-spin states.

may be understood by consideration of the fact that both the $B(M1)_{\mathrm{In}}$ and the $B(M1)_{\mathrm{Out}}$ values are sensitive to a change of structure in the wave functions and that both values are small after all. It is known that in ^{128}Cs and ^{130}Cs the staggering patterns of the experimental $B(M1)_{\mathrm{In}}/B(M1)_{\mathrm{Out}}$ ratios are in phase with those of the $B(M1)/B(E2)$ ratios for the yrast states [35]. The present calculation supports this experimental fact.

D. $E2$ and $M1$ band structures

To clarify the band structure with the $\nu h_{11/2} \otimes \pi h_{11/2}$ configuration, we calculate absolute values of $B(E2; I \to I-2)$ and $B(M1; I \to I-1)$ in the following text. In Fig. 9, the calculated $B(E2)$ values of the yrast and the yrare states are shown as functions of spin I. All the nuclei have the similar behavior of the $B(E2)$ values for the transitions between the even-spin yrast states ($I \geqslant 10$) and between the odd-spin yrast states ($I \geqslant 11$). The strong $E2$ transitions with spins greater than 12 indicate that the odd-spin and the even-spin yrast

states, respectively, form two $\Delta I = 2$ bands starting from the bandhead states of 11_1^+ and 10_1^+.

The $B(E2)$ values between the yrare $\Delta I = 2$ states are smaller than those between the yrast $\Delta I = 2$ states. However, because the yrare states are linked by the strong $E2$ transitions between the $\Delta I = 2$ states, quadrupole collectivity plays an important role in describing the even-spin and the odd-spin yrare states for $I > 11$. In ^{132}Cs it is not easy to identify which of the 15_2^+ and 15_3^+ states belongs to the $E2$ band, starting from the bandhead state of 9_1^+. The $B(E2; 15_3^+ \rightarrow 13_2^+)$ value of 0.0337 e^2b^2 is close to that of the $15_2^+ \rightarrow 13_2^+$ transition (0.0377 e^2b^2), and the 15_3^+ state is also a candidate as a member of the $\Delta I = 2$ band. Concerning the transitions from the yrare states to the yrast states, the $B(E2; 11_2^+ \rightarrow 9_1^+)$ and $B(E2; 10_2^+ \rightarrow 8_1^+)$ values are the largest compared with other transitions for all the nuclei ^{130}Cs, ^{132}Cs, ^{132}La, and ^{134}La.

On the basis of the preceding argument, we conclude that, for any nucleus, the following members form five $\Delta I = 2$ $E2$ bands, each starting from the first member as the bandhead state: (1) $11_1^+, 13_1^+, 15_1^+, 17_1^+$; (2) $10_1^+, 12_1^+, 14_1^+, 16_1^+$; (3) $9_1^+, 11_2^+, 13_2^+, 15_2^+$ (15_2^+ or 15_3^+ for ^{132}Cs); (4) $12_2^+, 14_2^+, 16_2^+$; and (5) $8_1^+, 10_2^+, 12_3^+$ (12_4^+ for ^{132}Cs and ^{134}La).

The calculated $B(M1)$ values of the yrast and the yrare states for ^{132}Cs, ^{130}Cs, ^{134}La, and ^{132}La are shown as functions of spin I in Fig. 10. For the yrast states of all the nuclei, the $B(M1)$ values ($I \geqslant 11$) are large for the transitions from odd spin to even spin and small for the transitions from even spin to odd spin. On the other hand, all the $B(M1)$ values between the yrare states ($I \geqslant 12$) are found to be small for any nucleus. This fact implies that the structure of the yrare band differs from that of the yrast band. Furthermore, with respect to the other $\Delta I = 1$ transitions, large $B(M1)$ values ($\geqslant 0.40\,\mu_N^2$) are predicted for the $10_1^+ \rightarrow 9_1^+ \rightarrow 8_1^+$, $12_1^+ \rightarrow 11_2^+ \rightarrow 10_2^+$, $14_1^+ \rightarrow 13_2^+$, and $16_1^+ \rightarrow 15_2^+$ transitions in ^{130}Cs, ^{134}La, and ^{132}La ($16_1^+ \rightarrow 15_3^+$ for ^{132}Cs). [$B(M1; 16_1^+ \rightarrow 15_3^+) = 1.67\mu_N^2$ for ^{132}Cs.]

The preceding results concerning $M1$ transitions are summarized as follows. The strong $M1$ transitions ($I \geqslant 11$) connect the odd-spin yrast states (I) to the even-spin yrast states ($I-1$), connect these ($I-1$) states to the odd-spin states ($I-2$), and connect these ($I-2$) states to the even spin states ($I-3$). These large $B(M1)$ values indicate that the $\Delta I = 1$ $M1$ bands are composed of the following four level sequences: (1) $8_1^+, 9_1^+, 10_1^+, 11_1^+$; (2) $10_2^+, 11_2^+, 12_1^+, 13_1^+$; (3) $13_2^+, 14_1^+, 15_1^+$; and (4) 15_2^+ (15_3^+ for ^{132}Cs), $16_1^+, 17_1^+$.

As an example, the partial level scheme of ^{134}La constructed from the results of the $M1$ and $E2$ transitions is shown in Fig. 11. We do not display other figures, but similar band schemes are deduced also for ^{132}Cs, ^{130}Cs, and ^{132}La. Our model gives five $\Delta I = 2$ bands with the bandhead states of $8_1^+, 9_1^+, 10_1^+, 11_1^+$, and 12_2^+. The states within four bands with the bandhead states of $8_1^+, 9_1^+, 10_1^+$, and 11_1^+ are connected by the strong $E2$ transitions to the same members of the $\Delta I = 2$ $E2$ bands and by the strong $M1$ transitions to the states in the neighboring $\Delta I = 2$ $E2$ bands. Here it should be mentioned that the structures of the even-spin yrare states ($12_2^+, 14_2^+, 16_2^+$) are quite different from those of the other $\Delta I = 2$ $E2$ bands,

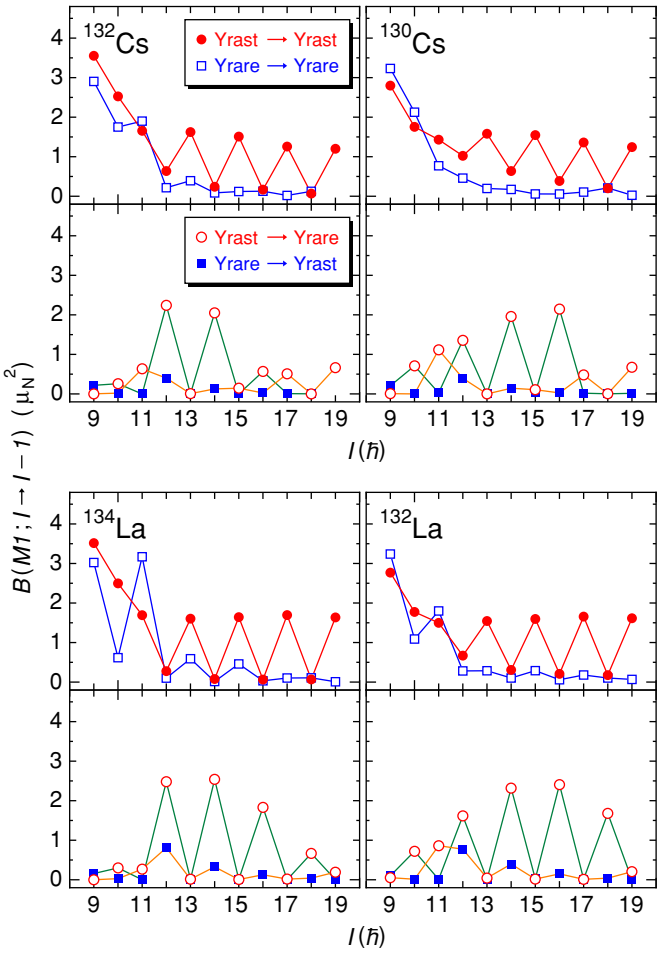

FIG. 10. (Color online). The theoretical $B(M1)$ values for ^{132}Cs, ^{130}Cs, ^{134}La, and ^{132}La.

as these states are not connected by the strong $M1$ transitions to any member of other $\Delta I = 2$ $E2$ bands.

The IBFFM approach [46] concluded that in ^{134}Pr the even-spin and the odd-spin yrast bands were based on the ground-state band of the even-even triaxial core and that the even-spin and the odd-spin yrare bands were based on the quasi-γ band. As for the yrast bands, the result is similar to ours. The PTSM shows that the odd-spin and the even-spin yrast states form two $\Delta I = 2$ $E2$ bands with the bandhead states of 11_1^+ and 10_1^+. However, in the PTSM, the odd-spin and even-spin yrare states are very different in their structure. The odd-spin yrare states, i.e., the 11_2^+, 13_2^+, and 15_2^+ states, form a $\Delta I = 2$ $E2$ band as the bandhead state of 9_1^+, whereas even-spin yrare states, i.e., the 12_2^+, 14_2^+ and 16_2^+ states, form a $\Delta I = 2$ $E2$ band as the bandhead state of 12_2^+. There exist very weak $E2$ transitions between the 10_2^+ and 12_2^+ states.

E. Microscopic origin

To search for the microscopic origin of the theoretical prediction of the large $M1$ transitions, we analyze the absolute values of reduced matrix elements of the $M1$ operator. The total reduced matrix elements M and the contributions from

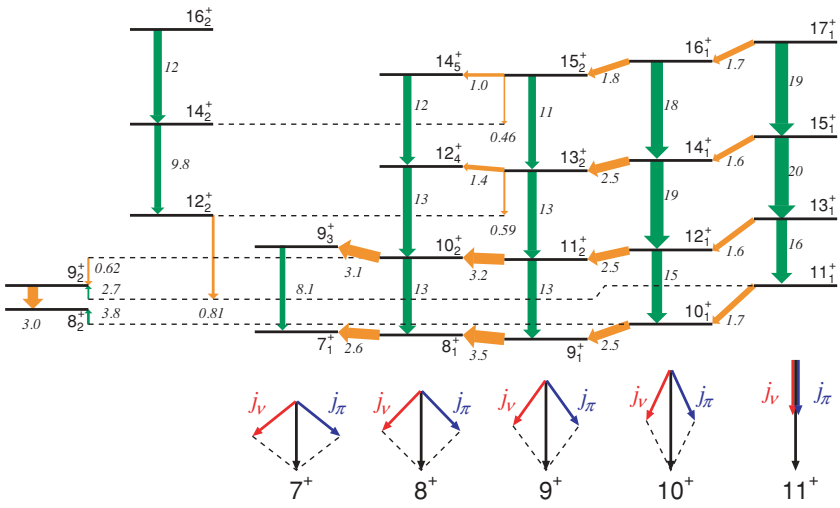

FIG. 11. (Color). Partial level scheme of ^{134}La suggested by the PTSM calculation. The width of the green arrows indicates the absolute $E2$ ($\Delta I = 2$) transition strengths [$B(E2) \geqslant 0.02\ e^2b^2$], and that of the orange arrows indicates the absolute $M1$ ($\Delta I = 1$) transition strengths [$B(M1) \geqslant 0.40\ \mu_N^2$]. The numerals on the right-hand side of the $E2$ transitions denote the $B(E2)$ values (in $10^{-2}\ e^2b^2$), and those beneath the $M1$ transitions denote the $B(M1)$ values (in μ_N^2). Schematic illustrations of the chopsticks configurations are presented below each $\Delta I = 2$ $E2$ band. The red and the blue arrows indicate the angular momenta of the neutron and the proton for the bandhead state, respectively. Their vector sum is indicated by black arrows. Four $\Delta I = 2$ bands and the band with the bandhead state of 7_1^+ have the configurations shown by the schematic illustrations below.

only the $0h_{11/2}$ orbitals M_j are defined as

$$M = |\langle \Phi(I\eta) \| T(M1) \| \Phi(I - 1\eta') \rangle|, \tag{19}$$

$$M_j = |\langle \Phi(I\eta) \| T_j(M1) \| \Phi(I - 1\eta') \rangle|, \tag{20}$$

where $T_j(M1)$ is the $M1$ transition operator acting on only the nucleons in the $0h_{11/2}$ orbital. Figure 12 shows the calculated values of M and M_j. It is seen that, for all the nuclei ^{130}Cs, ^{132}Cs, ^{132}La, and ^{134}La, the main contribution to the $M1$ matrix elements comes from the $0h_{11/2}$ orbitals.

To pin down their detailed microscopic origin, we consider a two-nucleon system of one neutron and one proton, both in the same $0h_{11/2}$ orbital. A detailed description is given in the appendix. From a simple geometrical consideration, the 8^+ state of the two-nucleon system is built by perpendicular

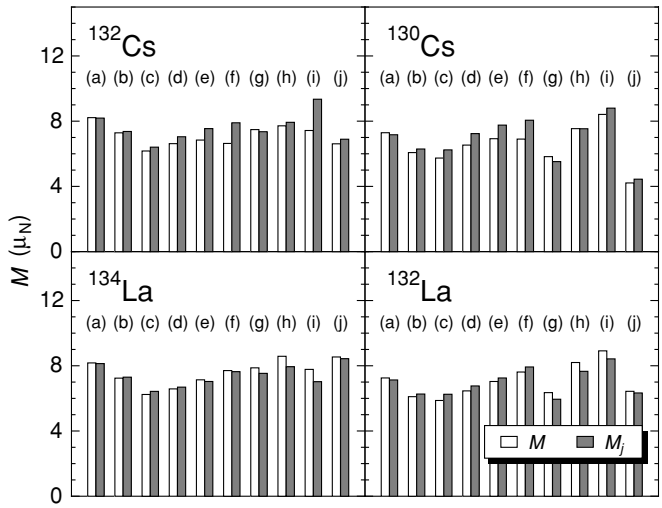

FIG. 12. Absolute values of reduced matrix elements of $M1$ operators: the total reduced matrix elements (M) and the contributions from only the $0h_{11/2}$ orbitals (M_j); (a) $9_1^+ \to 8_1^+$; (b) $10_1^+ \to 9_1^+$; (c) $11_1^+ \to 10_1^+$; (d) $13_1^+ \to 12_1^+$; (e) $15_1^+ \to 14_1^+$; (f) $17_1^+ \to 16_1^+$; (g) $12_1^+ \to 11_2^+$; (h) $14_1^+ \to 13_2^+$; (i) $16_1^+ \to 15_{2(3)}^+$ for ^{130}Cs, ^{134}La, and ^{132}La (for ^{132}Cs); (j) $11_2^+ \to 10_2^+$.

coupling of two angular momenta of the neutron and proton, whereas the 11^+ state is built by parallel coupling. The $B(M1)$ values are given by 1.5, 2.8, and 4.1 μ_N^2 for the $11^+ \to 10^+$, the $10^+ \to 9^+$, and the $9^+ \to 8^+$ transitions, respectively, as shown in Table II in the appendix. When these $B(M1)$ values are compared with those of the actual calculations for all the nuclei ^{130}Cs, ^{132}Cs, ^{132}La, and ^{134}La (see Fig. 10), it turns out that for $11 \leqslant I \leqslant 17$ the $B(M1)$ values from the odd-spin yrast states (I) to the even-spin yrast states ($I - 1$) are close to the two-nucleon $B(M1; 11^+ \to 10^+)$ value (1.5 μ_N^2).

Similarly, in ^{132}Cs and ^{134}La, the two-nucleon $B(M1; 10^+ \to 9^+)$ value (2.8 μ_N^2) is close to those from the even-spin yrast states ($I - 1$) to the odd-spin states ($I - 2$) except for the $B(M1; 16_1^+ \to 15_3^+)$ value (1.67 μ_N^2) in ^{132}Cs and the $B(M1; 16_1^+ \to 15_2^+)$ value (1.83 μ_N^2) in ^{134}La. The reduction of the $M1$ strengths comes from the mixing between the 15_2^+ and the 15_3^+ states, as we obtain the large $B(M1; 16_1^+ \to 15_2^+)$ value (0.568 μ_N^2) for ^{132}Cs and the $B(M1; 16_1^+ \to 15_3^+)$ value (1.29 μ_N^2) for ^{134}La. Concerning ^{130}Cs and ^{132}La, the behavior of the $B(M1)$ values from the even-spin yrast states ($I - 1$) to the odd-spin states ($I - 2$) is also analogous to that of ^{132}Cs and ^{134}La. However, the $B(M1)$ values of the $10_1^+ \to 9_1^+$ transition and the $12_1^+ \to 11_2^+$ transition for ^{130}Cs and ^{132}La are not so close to the two-nucleon $B(M1; 10^+ \to 9^+)$ value. This may be caused by the configuration mixing of the pure two-nucleon states with other states.

On the basis of the preceding considerations, the excitation mechanism of the doubly-odd nuclei in the mass $A \sim 130$ region can be interpreted in terms of the single-particle configurations of two angular momenta of the unpaired neutron and the unpaired proton, coupled with the quadrupole collective motion of the even-even core. Such single-particle configurations are called chopsticks configurations hereafter. The odd-spin yrast states (I) ($I \geqslant 11$) are the members of the $\Delta I = 2$ band with the bandhead state of 11_1^+, which has the parallel chopsticks configuration with angular momentum 11. Similarly, the yrast states of 10_1^+, 9_1^+, and 8_1^+ are built mainly from the chopsticks configurations with angular momenta 10, 9, and 8, respectively. In particular, the state 8_1^+ has the

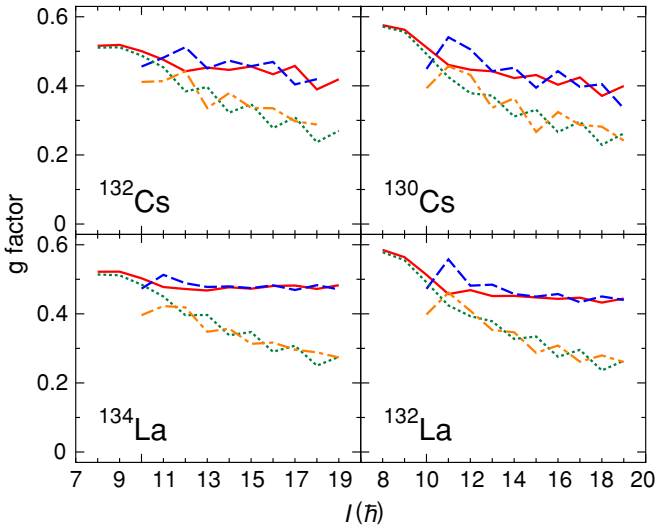

FIG. 13. (Color online). The calculated g factors in the PTSM. Solid curves indicate the g factors for the yrast states, and dashed curves indicate those for the yrare states; dotted curves indicate the g factors contributed from only the $0h_{11/2}$ orbitals for the yrast states, and dot-dashed curves indicate those for the yrare states.

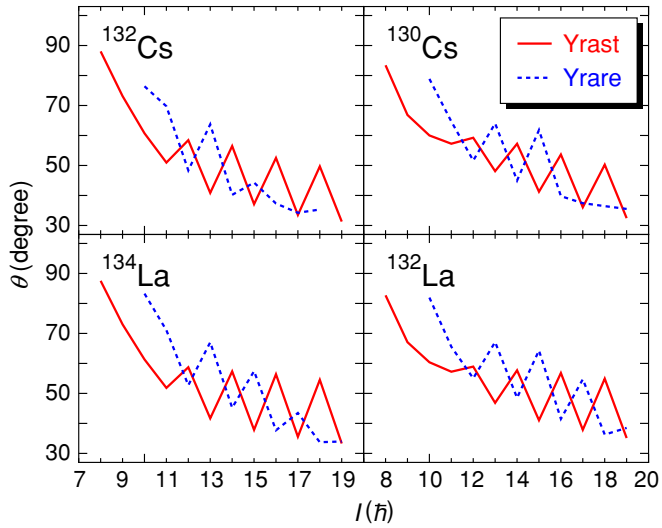

FIG. 14. (Color online). The effective angles of two angular momenta calculated in the PTSM. Solid curves indicate the effective angles for the yrast states, and dotted curves indicate those for the yrare states.

perpendicular chopsticks configuration. In the case of ^{134}La, the relation between the $\Delta I = 2$ $E2$ bands and the chopsticks configurations is presented in Fig. 11.

We conclude that, for all the nuclei ^{130}Cs, ^{132}Cs, ^{132}La, and ^{134}La, the basic structure of the $\Delta I = 2$ $E2$ bands is interpreted as arising from a weak coupling of the chopsticks configurations with the quadrupole collective excitations of the even-even part of the nucleus.

F. Magnetic moments

The g factors are calculated and predicted in the PTSM, although none of them are observed yet in experiment. The magnetic dipole operator is given by

$$\boldsymbol{\mu} = \mu_N \sum_{\tau=\nu,\pi} [g_{\ell\tau} \boldsymbol{j}_\tau + (g_{s\tau} - g_{\ell\tau}) \boldsymbol{s}_\tau], \tag{21}$$

where μ_N, $g_{\ell\tau}$, $g_{s\tau}$, $\boldsymbol{j}_\tau$, and $\boldsymbol{s}_\tau$ are as previously defined. The theoretical predictions for the g factors of the yrast and the yrare states are presented in Fig. 13, together with the g factors contributed from only the $0h_{11/2}$ orbitals. It is seen that for any nucleus the g factors are similar for the yrast and the yrare states. The mechanism of generating the magnetic moments changes with total spin I. In low-spin states such as the 8_1^+ state, the effect of the $0h_{11/2}$ orbitals is clearly dominant, but it gradually decreases as spin I increases. The rest is compensated for by the contribution from the core.

V. CHOPSTICKS MOTION AND CORE EXCITATIONS

A. Effective angles between proton and neutron angular momenta and squares of the core angular momentum

To deepen our understanding of the excitation mechanism of the yrast and yrare states with the $\nu h_{11/2} \otimes \pi h_{11/2}$ configuration, we calculate effective angles between two angular momenta of neutrons and protons in the $0h_{11/2}$ orbitals and squares of the core angular momentum. The effective angle θ is defined as

$$\cos\theta = \frac{\langle \Phi(I\eta)|\boldsymbol{j}_{\nu j} \cdot \boldsymbol{j}_{\pi j}|\Phi(I\eta)\rangle}{\sqrt{\langle \Phi(I\eta)|\boldsymbol{j}_{\nu j}^2|\Phi(I\eta)\rangle \langle \Phi(I\eta)|\boldsymbol{j}_{\pi j}^2|\Phi(I\eta)\rangle}}, \tag{22}$$

where the operator $\boldsymbol{j}_{\tau j}$ ($\tau = \nu$ or π) stands for the angular momentum operator of the nucleon in the $0h_{11/2}$ orbital. It should be mentioned that the effective angles never become zero because of quantum fluctuations, even though two angular momenta point toward the same direction. For example, we consider the two-nucleon system that consists of a neutron and a proton in the $0h_{11/2}$ orbitals. The effective angles turn out to be 32°, 57°, 75°, and 90° for the 11^+, 10^+, 9^+, and 8^+ states, respectively, as given by Table II in the appendix. Because a realistic nuclear state is expressed as a superposition of several configurations, the effective angles become larger than 32°.

The square of the core angular momentum $\langle \boldsymbol{R}^2 \rangle$ is defined as

$$\langle \boldsymbol{R}^2 \rangle = \langle \Phi(I\eta)|\boldsymbol{R}^2|\Phi(I\eta)\rangle, \tag{23}$$

where the core angular momentum operator $\boldsymbol{R}$ is defined by

$$\boldsymbol{R} = \boldsymbol{I} - \boldsymbol{j}_{\nu j} - \boldsymbol{j}_{\pi j}. \tag{24}$$

In Fig. 14, the effective angles θ for the yrast and yrare states of ^{130}Cs, ^{132}Cs, ^{132}La, and ^{134}La are shown as functions of spin I. The calculated values of $\langle \boldsymbol{R}^2 \rangle$ are plotted as functions of spin I in Fig. 15. We note the following facts: (1) For the 8_1^+ states of all the nuclei, two angular momenta of the neutrons and protons in the $0h_{11/2}$ orbitals are almost perpendicular to one another. The effective angles θ along the yrast states decrease monotonically as spin I increases up to spin 11. (2) The values of $\langle \boldsymbol{R}^2 \rangle$ for these states are close to each other (see Fig. 15), although their values are not zero because of a

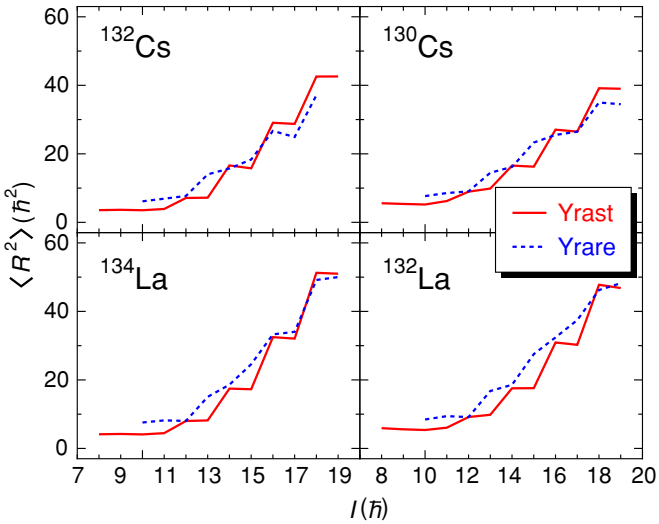

FIG. 15. (Color online). The squares of the core angular momentum calculated in the PTSM.

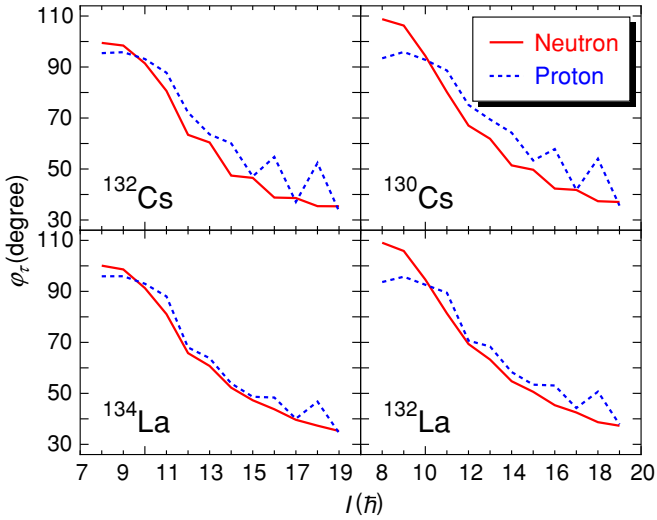

FIG. 16. (Color online). Effective angles of two angular momenta calculated in the PTSM for the yrast states. Solid and dotted curves indicate the effective angles between the core and the neutrons in the $0h_{11/2}$ orbitals and those between the core and protons, respectively.

small admixture of other angular momentum states. Thus it is inferred that the cores are made mainly of the 0^+ component, representing the ground state of the even-even core (even-even part of the nucleus). These two facts clearly show that the large interband $M1$ transitions in the yrast states for $I \leqslant 11$ come only from the closing of two angular momenta of the neutron and proton in the $0h_{11/2}$ orbitals.

The yrast states with spins greater than 11 exhibit the even-odd staggering of the effective angles θ, and their values are smaller than 60°. Considering the fact that the 10^+ state of the pure two-nucleon system has a near-parallel configuration of two angular momenta ($\theta = 57°$), in these four nuclei two angular momenta point toward almost the same direction, and repeat the opening and closing movement with a small difference in their angle (by only one unit in spin). In Fig. 15 the values of $\langle \boldsymbol{R}^2 \rangle$ show staircaselike behavior. Because the values of $\langle \boldsymbol{R}^2 \rangle$ for the even-spin yrast states $(I-1)$ and the odd-spin yrast states (I) are close to one another, it is inferred that their even-even cores have the same structure. The strong interband $M1$ transitions from the states (I) to the states $(I-1)$ are interpreted to come from the closing of two angular momenta of the neutron and proton. In contrast, the values of $\langle \boldsymbol{R}^2 \rangle$ are different for the odd-spin yrast states (I) and the even-spin yrast states $(I+1)$. Although two angular momenta of the neutron and proton open for the transitions from the states $(I+1)$ to the states (I), the $M1$ transitions are basically hindered because their cores are different in structure and are almost orthogonal to one another. Therefore it is concluded that the even-odd staggering of the $B(M1)$ values arise from a combination of the configurations of the unpaired neutron and the unpaired proton in the $0h_{11/2}$ orbitals and the quadrupole collective excitations of the even-even cores.

The difference between the chiral scheme and that of the PTSM is stated as follows. In the picture of the chiral structure, the angular momenta of the unpaired nucleons are assumed to be always perpendicular to one another. In the PTSM case, a similar situation is realized for only the first excited states of 8^+ with the $\nu h_{11/2} \otimes \pi h_{11/2}$ configuration as the perpendicular coupling of two angular momenta of the unpaired nucleons, though the even-even core has very small angular momentum. However, the physical situation deviates from the chiral picture for the other high-spin states. In view of the chiral interpretation, the angular momentum of the even-even core also points toward a direction perpendicular to both angular momenta of the unpaired nucleons, and the left-handed and the right-handed chiral geometries can be formed from three angular momenta, which are all perpendicular. This implies that the unpaired neutron and the unpaired proton are strongly coupled to compose the characteristic configuration of their angular momenta, even for the high-spin yrast states. On the other hand, the PTSM provides a weak coupling of the unpaired nucleons both in the $0h_{11/2}$ orbitals with quadrupole collective excitations of the even-even core. This weak mutual coupling allows the chopsticks of two angular momenta of the unpaired nucleons to open and close repeatedly as spin goes up, and it produces the large-amplitude staggering of the $B(M1)/B(E2)$ ratios along the yrast level sequences.

B. Effective angles between core's and nucleons' angular momenta

The effective angle between the angular momenta of the core and the nucleons in the $0h_{11/2}$ orbitals φ_τ ($\tau = \pi$ or ν) is defined as

$$\cos\varphi_\tau = \frac{\langle \Phi(I\eta)|\boldsymbol{R}\cdot\boldsymbol{j}_{\tau j}|\Phi(I\eta)\rangle}{\sqrt{\langle \Phi(I\eta)|\boldsymbol{R}^2|\Phi(I\eta)\rangle\langle \Phi(I\eta)|\boldsymbol{j}_{\tau j}^2|\Phi(I\eta)\rangle}}. \quad (25)$$

In Fig. 16, the effective angles φ_τ for the yrast states of ^{130}Cs, ^{132}Cs, ^{132}La, and ^{134}La are shown as functions of spin I. Concerning the low-spin states, two angular momenta of the core and the neutrons in the $0h_{11/2}$ orbital and those of the core and the protons are roughly perpendicular to one another for all cases. However, because their core angular momenta R

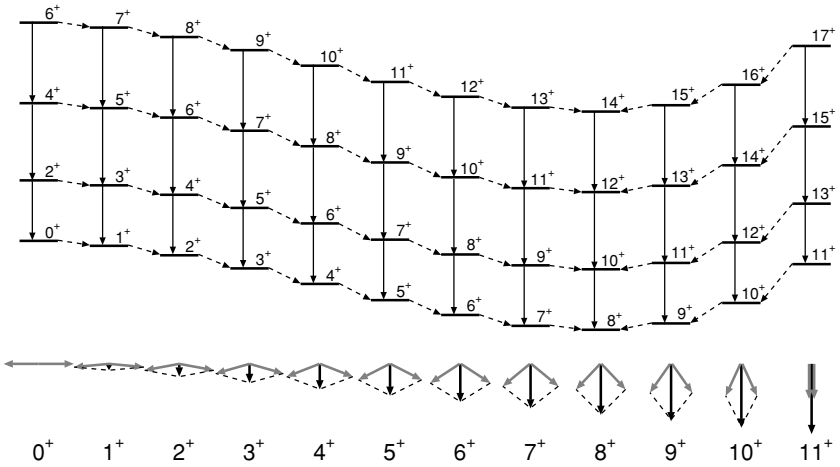

FIG. 17. Band scheme predicted by the PTSM calculation in the weak coupling limit. The narrow arrows indicate $E2$ transitions, and the dashed narrow arrows denote $M1$ transitions. Schematic illustrations of two angular momenta of the unpaired neutron and the unpaired proton are presented below the band scheme. The gray wide arrows indicate the angular momenta of the neutron and the proton. Their vector sum is indicated by black wide arrows. The $\Delta I = 2$ bands have the corresponding configurations shown by the schematic illustrations below (chopsticks configurations).

are very small compared with that of a high-spin yrast state with spins I greater than 14, their effective angles should have quantum fluctuations. Thus no definite argument is drawn for their mutual angle of the core and the nucleon angular momenta. With respect to the high-spin states ($I \geqslant 14$), the effective angles between two angular momenta of the core and the neutrons are smaller than 55° for any nucleus. The effective angles between two angular momenta of the core and the protons show the staggering pattern. As spin I increases, their average angles gradually decrease and reach the region where the effective angles are too small to avoid quantum fluctuations. The behavior of the effective angles suggests that two angular momenta of the core and the nucleon eventually point toward the same direction at high spin. Considering the effective angles between the neutron and the proton at high spin, it is surmised that the high-spin states are built by totally parallel coupling of three angular momenta of the even-even core, the unpaired neutron, and the unpaired proton in the $0h_{11/2}$ orbitals.

C. Schematic illustration

Our new interpretation leads to a schematic illustration of the band structure shown in Fig. 17, which is expected to occur in the weak coupling limit of the chopsticks configurations with the core excitations. The bandhead states of the $\Delta I = 2$ $E2$ bands are built on the unpaired nucleons both in the $0h_{11/2}$ orbitals, coupled with the even-even core of angular momentum 0. The spin of the bandhead states corresponds to one of the possible chopsticks configurations with angular momentum 0–11, whose schematic illustrations are shown below for each $\Delta I = 2$ $E2$ band in Fig. 17. In this schematic figure the $\Delta I = 2$ $E2$ bands are vertically formed, whereas the $\Delta I = 1$ $M1$ bands are horizontally formed. This is an ideal situation. In reality the configuration mixing washes away this ideal band structure, especially at high energy. In the actual calculations the PTSM provides four $\Delta I = 2$ $E2$ bands with the bandhead states of 8_1^+, 9_1^+, 10_1^+, and 11_1^+.

VI. SUMMARY AND CONCLUSIONS

In the present study we applied the PTSM to the calculation of the energy levels and the electromagnetic transitions for the yrast and the yrare states based on the $\nu h_{11/2} \otimes \pi h_{11/2}$ configuration in ^{130}Cs, ^{132}Cs, ^{132}La, and ^{134}La. The shell-model basis states were restricted to the SD pairs plus one-neutron and one-proton space. A prominent advantage of the PTSM is that even-even, odd-mass, and doubly-odd nuclei are treated on an equal footing. The effective Hamiltonian employed in this study consists of the single-particle energies and the $P+QQ$ interaction, whose strengths were determined so as to describe the energy levels of the even-even nuclei in a previous paper [23]. It is emphasized once again that we applied the same set of interactions fixed by the even-even nuclei to doubly-odd nuclei without any further modification.

For all the nuclei ^{130}Cs, ^{132}Cs, ^{132}La, and ^{134}La, our calculation reproduced quite well the experimental energy levels of the yrast and the yrare states. The PTSM also described well the large-amplitude staggering of the $B(M1)/B(E2)$ ratios for the yrast bands.

Through the analysis of electromagnetic transitions, it was confirmed that strong $M1$ transitions connect the odd-spin yrast states (I) ($I = 11, 13, 15, 17$) to the even-spin yrast states ($I - 1$) and connect these ($I - 1$) states to the odd-spin states ($I - 2$), and they form four $\Delta I = 1$ $M1$ bands. To find the microscopic origin of the electromagnetic properties, we calculated the two different kinds of reduced matrix elements of the $M1$ operator. We also compared the $B(M1)$ values for two-nucleon system with those of actual calculations. It turns out that the chopsticks motion of two angular momenta of the unpaired nucleons enhances the $B(M1)$ values and the odd-spin yrast states ($I \geqslant 11$) have their parallel configuration. Furthermore, the $E2$ character of the strong transitions indicates that four $\Delta I = 2$ $E2$ bands are formed starting from the 8_1^+, 9_1^+, 10_1^+, and 11_1^+ levels as the bandhead states, and their even-even cores have the quadrupole collective excitations.

The physical situation revealed in the preceding text is supported by further analyses, i.e., by calculation of the effective angles between two angular momenta of neutrons and protons in the $0h_{11/2}$ orbitals and the squares of the core angular momentum. The calculated effective angles show that the chopsticks of two angular momenta of the unpaired nucleons close with increasing spin I within each $\Delta I = 1$ $M1$ band. For the yrast states ($I \geqslant 11$), the chopsticks open and

close repeatedly as I increases, causing strong $M1$ transitions between the odd-spin states (I) and the even-spin states ($I-1$). However, there exist very weak transitions between the even-spin states ($I+1$) and the odd-spin states (I), as their cores are different in structure.

In conclusion, the experimentally identified yrast and yrare states with the $\nu h_{11/2} \otimes \pi h_{11/2}$ configuration in ^{130}Cs, ^{132}Cs, ^{132}La, and ^{134}La are interpreted as arising from the chopsticks configurations, which represent two angular momenta of the unpaired neutron and the unpaired proton, weakly coupled with the quadrupole collective excitations of the even-even core. The chopsticks motion along the yrast line ($I \geqslant 10$) provides the staggered strong $M1$ transitions. This new aspect arises naturally from our theoretical framework, which incorporates the intrinsic degrees of freedom of the core particles with the unpaired neutron and the unpaired proton.

ACKNOWLEDGMENTS

We thank Dr. T. Koike and Dr. M. Oi for their valuable discussions. K. H. thanks JSPS Research Fellowships for Young Scientists.

APPENDIX: TWO-PARTICLE STATE OF NEUTRON AND PROTON

In this appendix, we consider a two-nucleon system of one neutron and one proton in the same orbital j, where j symbolically represents the quantum numbers (n, ℓ, j). The wave function of the two-nucleon characterized by the total spin L and its projection M is written as

$$|\Phi(jj; LM)\rangle = \sum_{m_1 m_2} (jm_1 jm_2|LM)|jm_1\rangle_\nu |jm_2\rangle_\pi = [|j\rangle_\nu \otimes |j\rangle_\pi]^{(L)}_M, \quad \text{(A1)}$$

where $|jm\rangle_\tau$ ($\tau = \nu$ or π) denotes a single-particle state and (j, m) represents a set of quantum numbers necessary to specify the state (n, ℓ, j, m). Here, we adopt $j = 11/2$, $\ell = j - 1/2 = 5$, and $n = 0$ to represent the intruder orbital $0h_{11/2}$ in the 50–82 major shell.

1. Excitation energies

The matrix elements of the P+QQ interactions are given for the two-nucleon system in the following. We consider only the QQ interaction between neutrons and protons given by Eq. (15), as this is the only interaction that contributes to the excitation energies of the two-particle system for the Hamiltonian given by Eq. (9). Then the matrix element of the QQ interaction becomes

$$\langle \Phi(jj; LM)|H_{\nu\pi}|\Phi(jj; LM)\rangle = -\kappa_{\nu\pi}(-1)^{L+1} \begin{Bmatrix} j & j & L \\ j & j & 2 \end{Bmatrix} \langle j||Q_\nu||j\rangle_\nu \langle j||Q_\pi||j\rangle_\pi. \quad \text{(A2)}$$

TABLE II. Energies (in MeV), $B(M1; L \to L-1)$ values (in μ_N^2) and effective angles (in degrees) for two-nucleon system of one neutron and one proton.

L^π	Energy	$B(M1)$	Effective angle
0^+	4.11		180
1^+	3.77	6.5	166
2^+	3.11	7.6	156
3^+	2.19	7.9	146
4^+	1.11	7.7	136
5^+	−0.03	7.3	125
6^+	−1.06	6.8	114
7^+	−1.82	6.0	103
8^+	−2.10	5.1	90
9^+	−1.66	4.1	75
10^+	−0.23	2.8	57
11^+	2.49	1.5	32

Using the reduced matrix element of the quadrupole operator for a neutron or proton single-particle state,

$$\langle j||Q_\tau||j\rangle_\tau = \langle n\ell|r^2|n\ell\rangle \langle j||Y^{(2)}||j\rangle \quad \text{(A3)}$$

with

$$\langle n\ell|r^2|n\ell\rangle = \frac{1}{b^2}\left(2n + \ell + \frac{3}{2}\right) = \frac{j+1}{b^2}, \quad \text{(A4)}$$

$$\langle j||Y^{(2)}||j\rangle = \sqrt{\frac{5(2j+1)}{4\pi}}\left(j\tfrac{1}{2}20\middle|j\tfrac{1}{2}\right) = -\frac{1}{4}\sqrt{\frac{5(2j-1)(2j+1)(2j+3)}{4\pi j(j+1)}}, \quad \text{(A5)}$$

and

$$\begin{Bmatrix} j & j & L \\ j & j & 2 \end{Bmatrix} = -(-1)^L \frac{[3X(X+1) - 4j^2(j+1)^2]}{2(2j-1)j(j+1)(2j+1)(2j+3)} \quad \text{(A6)}$$

with

$$X = L(L+1) - 2j(j+1), \quad \text{(A7)}$$

we can rewrite Eq. (A2) as

$$\langle \Phi(jj; LM)|H_{\nu\pi}|\Phi(jj; LM)\rangle = -\kappa_{\nu\pi}\frac{5}{32\pi}\frac{(j+1)^2}{b^4}\left[\frac{3X(X+1)}{4j^2(j+1)^2} - 1\right]. \quad \text{(A8)}$$

The energies are numerically given in Table II with $\kappa_{\nu\pi} = -1.0$ and $b = 1$ and $j = 11/2$. A straightforward calculation gives the energy minimum at

$$L = \frac{\sqrt{8j^2 + 8j - 1} - 1}{2}. \quad \text{(A9)}$$

This gives $L \sim 8$ for $j = 11/2$.

2. $B(M1; L \to L-1)$ values

The $B(M1; L \to L-1)$ values are given for the two-particle state as follows. The reduced matrix element of the

$M1$ operator in Eq. (17) becomes

$$\begin{aligned}
&\langle\Phi(jj;L')||T(M1)||\Phi(jj;L)\rangle \\
&\quad=\mu_N\sqrt{(2L'+1)(2L+1)}(-1)^L\begin{Bmatrix} L & j & j \\ j & L' & 1\end{Bmatrix} \\
&\qquad\times\sqrt{\frac{3}{4\pi}}[(g_{s\nu}-g_{\ell\nu})\langle j||\boldsymbol{s}_\nu||j\rangle_\nu+g_{\ell\nu}\langle j||\boldsymbol{j}_\nu||j\rangle_\nu] \\
&\qquad+\mu_N\sqrt{(2L'+1)(2L+1)}(-1)^{L'}\begin{Bmatrix} L & j & j \\ j & L' & 1\end{Bmatrix} \\
&\qquad\times\sqrt{\frac{3}{4\pi}}[(g_{s\pi}-g_{\ell\pi})\langle j||\boldsymbol{s}_\pi||j\rangle_\pi+g_{\ell\pi}\langle j||\boldsymbol{j}_\pi||j\rangle_\pi].
\end{aligned} \tag{A10}$$

Using the reduced matrix element of a proton or neutron one-body state for orbital angular momentum and that of spin,

$$\langle j||\boldsymbol{j}_\tau||j\rangle_\tau=\sqrt{j(j+1)(2j+1)}, \tag{A11}$$

$$\begin{aligned}
\langle j||\boldsymbol{s}_\tau||j\rangle_\tau&=\frac{1}{2}\sqrt{\frac{2j+1}{j(j+1)}}\left[j(j+1)+\frac{3}{4}-\ell(\ell+1)\right] \\
&=\frac{1}{2}\sqrt{\frac{(2j+1)(j+1)}{j}},
\end{aligned} \tag{A12}$$

and

$$\begin{aligned}
&\begin{Bmatrix} L & j & j \\ j & L-1 & 1\end{Bmatrix} \\
&\quad=\frac{(-1)^{L+1}}{2}\sqrt{\frac{(2j+L+1)L(2j-L+1)}{(2L-1)(2L+1)j(2j+1)(j+1)}},
\end{aligned} \tag{A13}$$

we can express the $B(M1;L\to L-1)$ value as

$$\begin{aligned}
&B(M1;L\to L-1) \\
&\quad=\frac{1}{2L+1}|\langle\Phi(jj;L-1)||T(M1)||\Phi(jj;L)\rangle|^2 \\
&\quad=\frac{3}{16\pi}\mu_N^2\frac{L(2j+L+1)(2j-L+1)}{2L+1} \\
&\qquad\times\left|\frac{1}{2j}(g_{s\nu}-g_{\ell\nu}-g_{s\pi}+g_{\ell\pi})+(g_{\ell\nu}-g_{\ell\pi})\right|^2.
\end{aligned} \tag{A14}$$

The numerical values for $j=11/2$, $g_{\ell\nu}=0.00$, $g_{\ell\pi}=1.00$, $g_{s\nu}=-2.68$, and $g_{s\pi}=3.91$ are given in Table II.

3. Effective angles between neutron and proton angular momenta

Here we calculate the effective angle θ between the neutron and the proton angular momenta. The matrix element of the scalar product of neutron and proton angular momenta is

$$\begin{aligned}
&\langle\Phi(jj;LM)\left|\boldsymbol{j}_\nu\cdot\boldsymbol{j}_\pi\right|\Phi(jj;LM)\rangle \\
&\quad=(-1)^{L+1}\begin{Bmatrix} j & j & L \\ j & j & 1\end{Bmatrix}\langle j||\boldsymbol{j}_\nu||j\rangle_\nu\langle j||\boldsymbol{j}_\pi||j\rangle_\pi.
\end{aligned} \tag{A15}$$

Because of Eq. (A11) and

$$\begin{Bmatrix} j & j & L \\ j & j & 1\end{Bmatrix}=\frac{(-1)^{L+1}}{2}\frac{L(L+1)-2j(j+1)}{j(j+1)(2j+1)}, \tag{A16}$$

the matrix element is just given as

$$\begin{aligned}
&\langle\Phi(jj;LM)|\boldsymbol{j}_\nu\cdot\boldsymbol{j}_\pi|\Phi(jj;LM)\rangle \\
&\quad=\tfrac{1}{2}L(L+1)-j(j+1).
\end{aligned} \tag{A17}$$

Because the matrix element of the squared angular momentum operator of neutrons or protons becomes

$$\langle\Phi(jj;LM)|\boldsymbol{j}_\tau^2|\Phi(jj;LM)\rangle=j(j+1), \tag{A18}$$

the effective angle is given by

$$\cos\theta=\frac{L(L+1)}{2j(j+1)}-1. \tag{A19}$$

The numerical values of θ for $j=11/2$ are given in Table II.

4. Magnetic moments

The magnetic dipole moment of the two-particle state, $\mu(L)$, is defined as

$$\begin{aligned}
\mu(L)&=\langle\Phi(jj;LL)|\boldsymbol{\mu}_{m=0}|\Phi(jj;LL)\rangle \\
&=\sqrt{\frac{L}{(L+1)(2L+1)}}\langle\Phi(jj;L)||\boldsymbol{\mu}||\Phi(jj;L)\rangle.
\end{aligned} \tag{A20}$$

Using the relation between the magnetic dipole operator and the $M1$ transition operator,

$$\boldsymbol{\mu}=\sqrt{\frac{4\pi}{3}}T(M1), \tag{A21}$$

and Eqs. (A10)–(A12), we can express the magnetic dipole moment as

$$\mu(L)=\frac{\mu_N L}{2}\left[\frac{1}{2j}(g_{s\nu}-g_{\ell\nu}+g_{s\pi}-g_{\ell\pi})+(g_{\ell\nu}+g_{\ell\pi})\right]. \tag{A22}$$

5. Quadrupole moments

The electric quadrupole moment of the two-particle state, $Q(L)$, is written as

$$\begin{aligned}
Q(L)&=\langle\Phi(jj;LL)|Q_{m=0}|\Phi(jj;LL)\rangle \\
&=\sqrt{\frac{L(2L-1)}{(L+1)(2L+1)(2L+3)}} \\
&\quad\times\langle\Phi(jj;L)||Q||\Phi(jj;L)\rangle.
\end{aligned} \tag{A23}$$

Here, the electric quadrupole operator is given by

$$Q=\frac{1}{e}\sqrt{\frac{16\pi}{5}}(e_\nu Q_\nu+e_\pi Q_\pi), \tag{A24}$$

where e_τ and Q_τ are as previously defined. Using Eqs. (A3)–(A5), we can express the reduced matrix element of the quadrupole operator as

$$\langle \Phi(jj;L)||Q||\Phi(jj;L)\rangle = -\frac{e_\nu + e_\pi}{4eb^2}\sqrt{\frac{L(L+1)(2L+1)}{(2L-1)(2L+3)}} \times \frac{3[L(L+1)-1]-4j(j+1)}{j}. \quad \text{(A25)}$$

Thus, the electric quadrupole moment is given by

$$Q(L) = -\frac{e_\nu + e_\pi}{4eb^2}\frac{L}{2L+3} \times \frac{3[L(L+1)-1]-4j(j+1)}{j}. \quad \text{(A26)}$$

[1] G. Puddu, O. Scholten, and T. Otsuka, Nucl. Phys. **A348**, 109 (1980).
[2] R. F. Casten and P. von Brentano, Phys. Lett. **B152**, 22 (1985).
[3] D. Husar, S. J. Mills, H. Gräf, U. Neumann, D. Pelte, and G. Seiler-Clark, Nucl. Phys. **A292**, 267 (1977).
[4] H. Kusakari, K. Kitao, K. Sato, M. Sugawara, and H. Katsuragawa, Nucl. Phys. **A401**, 445 (1983).
[5] A. Dewald, S. Harissopulos, G. Böhm, A. Gelberg, K. P. Schmittgen, R. Wirowski, K. O. Zell, and P. von Brentano, Phys. Rev. C **37**, 289 (1988).
[6] S. Juutinen, S. Törmänen, P. Ahonen, M. Carpenter, C. Fahlander, J. Gascon, R. Julin, A. Lampinen, T. Lönnroth, J. Nyberg, A. Pakkanen, M. Piiparinen, K. Schiffer, P. Šimeček, G. Sletten, and A. Virtanen, Phys. Rev. C **52**, 2946 (1995).
[7] J. Genevey, J. A. Pinston, C. Foin, M. Rejmund, R. F. Casten, H. Faust, and S. Oberstedt, Phys. Rev. C **63**, 054315 (2001).
[8] J. J. Valiente-Dobón, P. H. Regan, C. Wheldon, C. Y. Wu, N. Yoshinaga, K. Higashiyama, J. F. Smith, D. Cline, R. S. Chakrawarthy, R. Chapman, M. Cromaz, P. Fallon, S. J. Freeman, A. Görgen, W. Gelletly, A. Hayes, H. Hua, S. D. Langdown, I. Y. Lee, X. Liang, A. O. Macchiavelli, C. J. Pearson, Zs. Podolyk, G. Sletten, R. Teng, D. Ward, D. D. Warner, and A. D. Yamamoto, Phys. Rev. C **69**, 024316 (2004).
[9] T. Shizuma, Z. G. Gan, K. Ogawa, H. Nakada, M. Oshima, Y. Toh, T. Hayakawa, Y. Hatsukawa, M. Sugawara, Y. Utsuno, and Z. Liu, Eur. Phys. J. A **20**, 207 (2004).
[10] F. Iachello and A. Arima, *The Interacting Boson Model* (Cambridge University Press, Cambridge, 1987).
[11] R. F. Casten, P. von Brentano, K. Heyde, P. Van Isacker, and J. Jolie, Nucl. Phys. **A439**, 289 (1985).
[12] A. Sevrin, K. Heyde, and J. Jolie, Phys. Rev. C **36**, 2631 (1987).
[13] X. W. Pan, T. Otsuka, J. Q. Chen, and A. Arima, Phys. Lett. **B287**, 1 (1992).
[14] T. Otsuka, Nucl. Phys. **A557**, 531c (1993).
[15] T. Mizusaki and T. Otsuka, Prog. Theor. Phys. Suppl. **125**, 97 (1996).
[16] O. Vogel, P. Van Isacker, A. Gelberg, P. von Brentano, and A. Dewald, Phys. Rev. C **53**, 1660 (1996).
[17] N. Yoshinaga, Nucl. Phys. **A503**, 65 (1989).
[18] N. Yoshinaga and D. M. Brink, Nucl. Phys. **A515**, 1 (1990).
[19] N. Yoshinaga, Nucl. Phys. **A570**, 421 (1994).
[20] N. Yoshinaga, T. Mizusaki, A. Arima, and Y. D. Devi, Prog. Theor. Phys. Suppl. **125**, 65 (1996).
[21] N. Yoshinaga, Y. D. Devi, and A. Arima, Phys. Rev. C **62**, 024309 (2000).
[22] K. Higashiyama, N. Yoshinaga, and K. Tanabe, Phys. Rev. C **67**, 044305 (2003).
[23] N. Yoshinaga and K. Higashiyama, Phys. Rev. C **69**, 054309 (2004).
[24] T. Takahashi, N. Yoshinaga, and K. Higashiyama, Phys. Rev. C **71**, 014305 (2005).
[25] P. R. Sala, N. Blasi, G. LoBianco, A. Mazzoleni, R. Reinhardt, K. Schiffer, K. P. Schmittgen, G. Siems, and P. von Brentano, Nucl. Phys. **A531**, 383 (1991).
[26] T. Hayakawa, J. Lu, K. Furuno, K. Furutaka, T. Komatsubara, T. Shizuma, N. Hasimoto, T. Saitoh, M. Kidera, Y. Hatsukawa, and M. Oshima, Z. Phys. A **357**, 349 (1997).
[27] Y. Khazov, A. A. Rodionov, S. Sakharov, and B. Singh, Nucl. Data Sheets **104**, 497 (2005).
[28] V. Kumar, P. Das, R. P. Singh, S. Muralithar, and R. K. Bhowmik, Eur. Phys. J. A **17**, 153 (2003).
[29] K. Starosta, T. Koike, C. J. Chiara, D. B. Fossan, D. R. LaFosse, A. A. Hecht, C. W. Beausang, M. A. Caprio, J. R. Cooper, R. Krücken, J. R. Novak, N. V. Zamfir, K. E. Zyromski, D. J. Hartley, D. Balabanski, J. Y. Zhang, S. Frauendorf, and V. I. Dimitrov, Phys. Rev. Lett. **86**, 971 (2001).
[30] A. A. Hecht, C. W. Beausang, K. E. Zyromski, D. L. Balabanski, C. J. Barton, M. A. Caprio, R. F. Casten, J. R. Cooper, D. J. Hartley, R. Krücken, D. Meyer, H. Newman, J. R. Novak, E. S. Paul, N. Pietralla, A. Wolf, N. V. Zamfir, Jing-Ye Zhang, and F. Dönau, Phys. Rev. C **63**, 051302(R) (2001).
[31] T. Koike, K. Starosta, C. J. Chiara, D. B. Fossan, and D. R. LaFosse, Phys. Rev. C **63**, 061304(R) (2001).
[32] D. J. Hartley, L. L. Riedinger, M. A. Riley, D. L. Balabanski, F. G. Kondev, R. W. Laird, J. Pfohl, D. E. Archer, T. B. Brown, R. M. Clark, M. Devlin, P. Fallon, I. M. Hibbert, D. T. Joss, D. R. LaFosse, P. J. Nolan, N. J. O'Brien, E. S. Paul, D. G. Sarantites, R. K. Sheline, S. L. Shepherd, J. Simpson, R. Wadsworth, Jing-ye Zhang, P. B. Semmes, and F. Dönau, Phys. Rev. C **64**, 031304(R) (2001).
[33] R. A. Bark, A. M. Baxter, A. P. Byrne, G. D. Dracoulis, T. Kibédi, T. R. McGoram, and S. M. Mullins, Nucl. Phys. **A691**, 577 (2001).
[34] K. Starosta, C. J. Chiara, D. B. Fossan, T. Koike, T. T. S. Kuo, D. R. LaFosse, S. G. Rohoziński, Ch. Droste, T. Morek, and J. Srebrny, Phys. Rev. C **65**, 044328 (2002).
[35] T. Koike, K. Starosta, C. J. Chiara, D. B. Fossan, and D. R. LaFosse, Phys. Rev. C **67**, 044319 (2003).
[36] G. Rainovski, E. S. Paul, H. J. Chantler, P. J. Nolan, D. G. Jenkins, R. Wadsworth, P. Raddon, A. Simons, D. B. Fossan, T. Koike, K. Starosta, C. Vaman, E. Farnea, A. Gadea, Th. Kröll, R. Isocrate, G. de Angelis, D. Curien, and V. I. Dimitrov, Phys. Rev. C **68**, 024318 (2003).

[37] A. A. Hecht, C. W. Beausang, H. Amro, C. J. Barton, Z. Berant, M. A. Caprio, R. F. Casten, J. R. Cooper, D. J. Hartley, R. Krücken, D. A. Meyer, H. Newman, J. R. Novak, N. Pietralla, J. J. Ressler, A. Wolf, N. V. Zamfir, Jing-Ye Zhang, and K. E. Zyromski, Phys. Rev. C **68**, 054310 (2003).
[38] S. Frauendorf and J. Meng, Nucl. Phys. **A617**, 131 (1997).
[39] V. I. Dimitrov, S. Frauendorf, and F. Dönau, Phys. Rev. Lett. **84**, 5732 (2000).
[40] J. Peng, J. Meng, and S. Q. Zhang, Phys. Rev. C **68**, 044324 (2003).
[41] T. Koike, K. Starosta, and I. Hamamoto, Phys. Rev. Lett. **93**, 172502 (2004).
[42] F. Iachello and P. Van Isacker, *The Interacting Boson-Fermion Model* (Cambridge University Press, Cambridge, 1991).
[43] D. Bucurescu, D. Barnéoud, Gh. Căta-Danil, T. von Egidy, J. Genevey, A. Gizon, J. Gizon, C. F. Liang, P. Paris, B. Weiss, S. Brant, V. Paar, and R. Pezer, Nucl. Phys. **A587**, 475 (1995).
[44] C. M. Petrache, C. A. Ur, D. Bazzacco, S. Lunardi, C. Rossi Alvarez, M. Ionescu-Bujor, A. Iordachescu, D. Bucurescu, F. Brandolini, G. de Angelis, G. Maron, D. R. Napoli, P. Pavan, N. H. Medina, R. Venturelli, S. Brant, and D. Vretenar, Nucl. Phys. **A603**, 50 (1996).
[45] C. M. Petrache, S. Brant, D. Bazzacco, G. Falconi, E. Farnea, S. Lunardi, V. Paar, Zs. Podolyák, R. Venturelli, and D. Vretenar, Nucl. Phys. **A635**, 361 (1998).
[46] S. Brant, D. Vretenar, and A. Ventura, Phys. Rev. C **69**, 017304 (2004).
[47] N. Yoshinaga and K. Higashiyama, in *Symmetries in Science XI*, edited by B. J. Gruber, G. Marmo, and N. Yoshinaga, (Kluwer Academic, Dordrecht, 2004), p. 589.
[48] K. Higashiyama and N. Yoshinaga, Prog. Theor. Phys. **113**, 1139 (2005).
[49] K. Higashiyama and N. Yoshinaga, in *A New Era of Nuclear Structure Physics*, edited by Y. Suzuki, S. Ohya, M. Matsuo, and T. Ohtsubo (World Scientific, Singapore, 2004), p. 338.
[50] N. Yoshinaga and K. Higashiyama, J. Phys. G (to be published).
[51] B. Fogelberg and J. Blomqvist, Nucl. Phys. **A429**, 205 (1984).
[52] M. Sanchez-Vega, B. Fogelberg, H. Mach, R. B. E. Taylor, A. Lindroth, J. Blomqvist, A. Covello, and A. Gargano, Phys. Rev. C **60**, 024303 (1999).
[53] W. J. Baldridge, Phys. Rev. C **18**, 530 (1978).
[54] C. Girit, W. D. Hamilton, and E. Michelakakis, J. Phys. G **6**, 1025 (1980).
[55] L. Goettig, Ch. Droste, A. Dygo, T. Morek, J. Srebrny, R. Broda, J. Styczeń, J. Hattula, H. Helppi, and M. Jääskeläinen, Nucl. Phys. **A357**, 109 (1981).
[56] T. Morek, H. Beuscher, B. Bochev, D. R. Haenni, R. M. Lieder, T. Kutsarova, M. Müller-Veggian, and A. Neskakis, Z. Phys. A **298**, 267 (1980).
[57] B. Fazekas, T. Belgya, G. Molnár, Á. Veres, R. A. Gatenby, S. W. Yates, and T. Otsuka, Nucl. Phys. **A548**, 249 (1992).
[58] T. Morek, H. Beuscher, B. Bochev, T. Kutsarova, R. M. Lieder, M. Müller-Veggian, and A. Neskakis, Nucl. Phys. **A433**, 159 (1985).
[59] A. A. Sonzogni, Nucl. Data Sheets **103**, 1 (2004).
[60] A. Bohr and B. Mottelson, *Nuclear Structure* (Benjamin, New York, 1975), Vol. 1.
[61] C. M. Petrache, D. Bazzacco, S. Lunardi, C. Rossi Alvarez, G. de Angelis, M. De Poli, D. Bucurescu, C. A. Ur, P. B. Semmes, and R. Wyss, Nucl. Phys. **A597**, 106 (1996).